CHAPTER IV

RESULTS AND DISCUSSION

4.1 Synthesis of Metal-Amine and Mixed Metal-Amine Complexes

Metal-amine and mixed-metal amine complexes were synthesized by using different solvents. In the first method, acetone was used as the solvent to synthesize metal-amine complexes and mixed metal-amine complexes between metal (II) acetate and tetraethylenepentamine (tetraen) as shown in Scheme 4.1. The solvent was evaporated and the metal complexes were dried under vacuum. All complexes were obtained as viscous liquid.

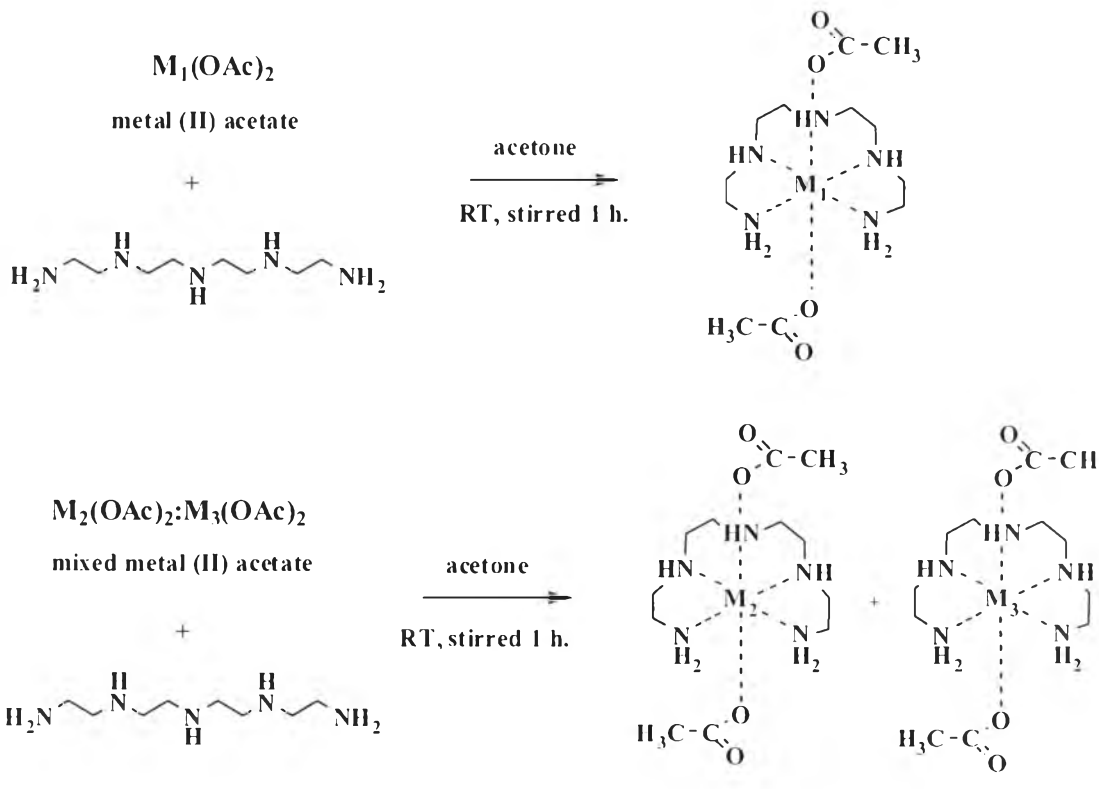

Scheme 4.1 Synthesis of metal-amine and mixed metal-amine complexes

(M_1 = Cu, Zn, Ni, Co and Mn; M_2 = Cu, M_3 = Zn, Ni, Co and Mn)

In the second method, water was used as solvent and blowing agent. Metal (II) acetate, tetraen and surfactant were stirred in water for 1 hour. A solution containing metal complex was then used for preparing rigid polyurethane foams.

4.2 Characterization of Metal-Amine and Mixed Metal-Amine Complexes

4.2.1 Characterization of Copper-Amine Complex

4.2.1.1 IR Spectroscopy of $Cu(OAc)_2$(tetraen) Complex

IR spectra of $Cu(OAc)_2$, tetraen and $Cu(OAc)_2$(tetraen) are shown in Figure 4.1. N-H stretching, C-H stretching and C-N stretching of $Cu(OAc)_2$(tetraen) were observed at 3137-3251 cm^{-1}, 2930 cm^{-1} and 1334 cm^{-1}, respectively. They shifted from N-H stretching, C-H stretching and C-N stretching of tetraen, which appeared at 3184-3354 cm^{-1}, 2936 cm^{-1} and 1323 cm^{-1}, respectively. The C=O stretching of carbonyl group in $Cu(OAc)_2$(tetraen) appeared at 1557 cm^{-1} (asymmetric C=O) and 1392 cm^{-1} (symmetric C=O), which were different from those of $Cu(OAc)_2$ normally appears at 1589 cm^{-1} (asymmetric C=O) and 1416 cm^{-1} (symmetric C=O). C-O stretching of $Cu(OAc)_2$(tetraen) was observed at 1007 cm^{-1} which shifted from that of $Cu(OAc)_2$ at 1032 cm^{-1}. It was indicated that the IR peaks of $Cu(OAc)_2$(tetraen) shifted from those $Cu(OAc)_2$ which confirmed that the complex was formed.

4.2.1.2 UV-Visible Spectroscopy of $Cu(OAc)_2$(tetraen) Complex

The complex formation was confirmed using UV-visible spectroscopy. UV-visible spectra of $Cu(OAc)_2$, $Cu(OAc)_2$(tetraen) and $Cu(OAc)_2$(tetraen)-W are shown in Figure 4.2. $Cu(OAc)_2$ has a strong absorption at 244 nm. UV-visible spectra of $Cu(OAc)_2$(tetraen) and $Cu(OAc)_2$(tetraen)-W synthesized in acetone and water, respectively, were compared. Both $Cu(OAc)_2$(tetraen) and $Cu(OAc)_2$(tetraen)-W gave the same absorption at 264 nm. It was indicated that $Cu(OAc)_2$(tetraen) complex could be obtained by using acetone and water in the synthesis because their UV peaks shifted from typical maximum absorption of $Cu(OAc)_2$.

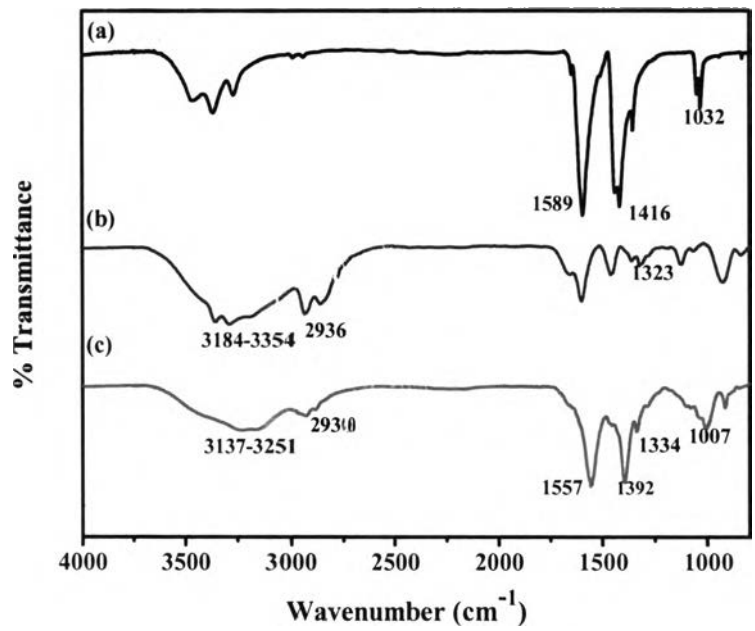

Figure 4.1 IR spectra of (a) $Cu(OAc)_2$; (b) tetraen; (c) $Cu(OAc)_2$(tetraen)

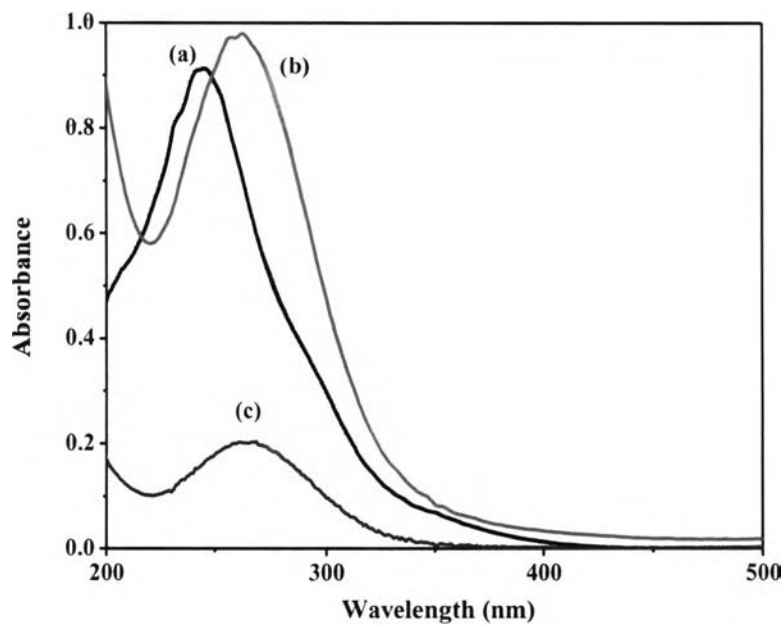

Figure 4.2 UV spectra of (a) $Cu(OAc)_2$; (b) $Cu(OAc)_2$(tetraen); (c) $Cu(OAc)_2$(tetraen)-W

4.2.1.3 Analytical Characteristics of $Cu(OAc)_2$(tetraen) Complex

Elemental analysis (EA) was used to determine %C, %H and %N. Atomic absorption spectroscopy (AAS) was used to analyze of %metal in $Cu(OAc)_2$(tetraen) complex. The calculated results were different from experimental results (Table 4.1).

Table 4.1 Analytical characteristics of $Cu(OAc)_2$(tetraen) complex

Complex	Elements determined	Experimental (%)	Calculated (%)
$Cu(OAc)_2$(tetraen)	%Cu	14.70	17.12
($CuC_{12}O_4H_{29}N_5$)	%C	38.84	38.83
	%H	7.89	7.88
	%N	15.58	18.89

4.2.1.4 Mass Spectrometry (MS) of $Cu(OAc)_2$(tetraen) Complex

The molecular ion peak corresponding to $[^{63}Cu(OAc)_2(tetraen)+H]^+$ and $[^{65}Cu(OAc)_2(tetraen).H_2O+H]^+$ appear as the protonated form at *m/z* of 370.42 and 391.13, respecively (Table 4.2 and Figure 4.3). It was indicated that the complex of $Cu(OAc)_2$(tetraen) was formed.

Table 4.2 MS data of $Cu(OAc)_2$(tetraen) complex

Molecular ion	Found	Calculated
$[^{63}Cu(OAc)_2(tetraen)+H]^+$	370.42	370.96
$[^{65}Cu(OAc)_2(tetraen).H_2O+H]^+$	391.13	391.17

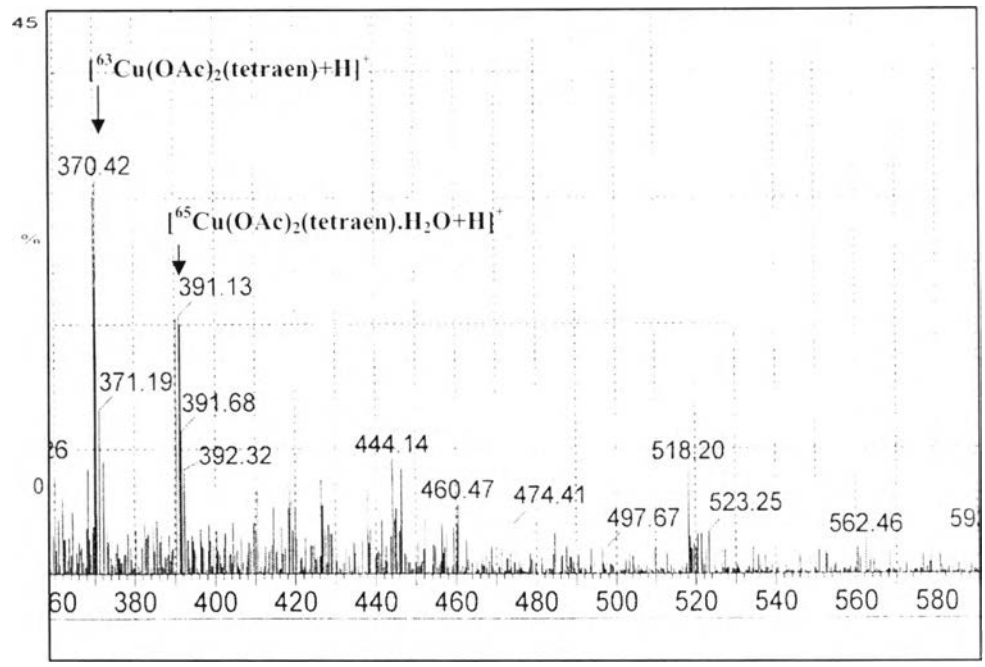

Figure 4.3 Mass spectrum of $Cu(OAc)_2$(tetraen) complex

4.2.2 Characterization of Zinc-Amine Complex

4.2.2.1 IR Spectroscopy of $Zn(OAc)_2$(tetraen) Complex

IR spectra of $Zn(OAc)_2$, tetraen and $Zn(OAc)_2$(tetraen) are shown in Figure 4.4. N-H stretching, C-H stretching and C-N stretching of $Zn(OAc)_2$(tetraen) were observed at 3163-3289 cm^{-1}, 2927 cm^{-1} and 1331 cm^{-1}, respectively. They shifted from N-H stretching, C-H stretching and C-N stretching of tetraen, which appeared at 3184-3354 cm^{-1}, 2936 cm^{-1} and 1323 cm^{-1}, respectively. The C=O stretching of carbonyl group in $Zn(OAc)_2$(tetraen) appeared at 1562 cm^{-1} (asymmetric C=O) and 1388 cm^{-1} (symmetric C=O), which were different from those of $Zn(OAc)_2$ normally appears at 1549 cm^{-1} (asymmetric C=O) and 1434 cm^{-1} (symmetric C=O) [33]. C-O stretching of $Zn(OAc)_2$(tetraen) was observed at 1003 cm^{-1} which shifted from that of $Zn(OAc)_2$ at 1017 cm^{-1}. It was indicated that the IR peaks of $Zn(OAc)_2$(tetraen) shifted from those $Zn(OAc)_2$ which confirmed that the complex was formed.

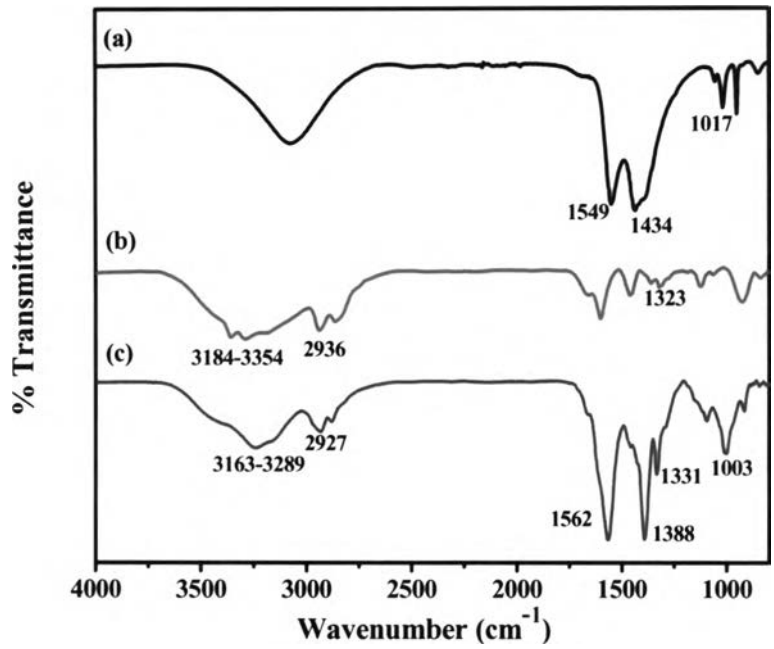

Figure 4.4 IR spectra of (a) $Zn(OAc)_2$; (b) tetraen; (c) $Zn(OAc)_2$(tetraen)

4.2.2.2 UV-visible Spectroscopy of $Zn(OAc)_2$(tetraen) Complex

UV-visible spectra of $Zn(OAc)_2$, $Zn(OAc)_2$(tetraen) and $Zn(OAc)_2$(tetraen)-W are shown in Figure 4.5. $Zn(OAc)_2$ has the absorption at 201 nm. UV-visible spectra of $Zn(OAc)_2$(tetraen) and $Zn(OAc)_2$(tetraen)-W synthesized in acetone and water, respectively, were compared. Both $Zn(OAc)_2$(tetraen) and $Zn(OAc)_2$(tetraen)-W gave the same absorption at 203 nm. It was indicated that $Zn(OAc)_2$(tetraen) complex could be obtained by using acetone and water in the synthesis because their UV peaks shifted from typical maximum absorption of $Zn(OAc)_2$.

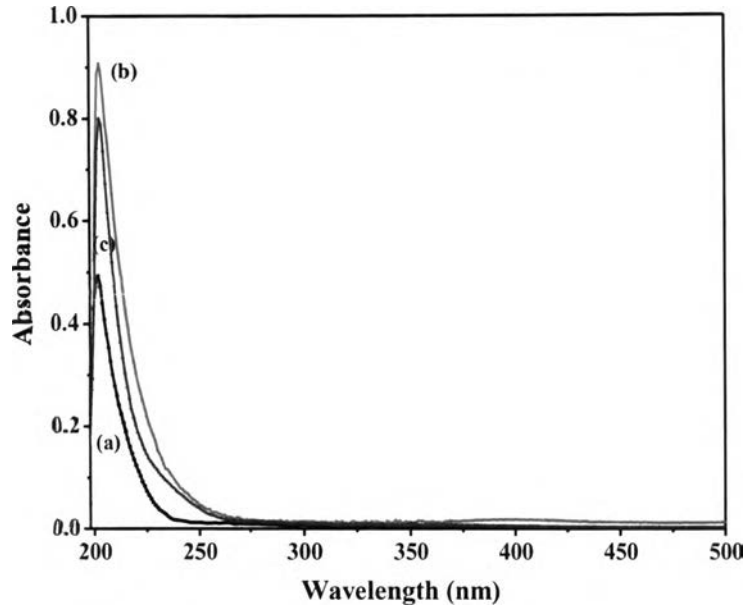

Figure 4.5 UV spectra of (a) $Zn(OAc)_2$; (b) Zn(tetraen); (c) $Zn(OAc)_2$(tetraen)-W

4.2.2.3 Analytical Characteristics of $Zn(OAc)_2$(tetraen) Complex

Elemental analysis (EA) was used to determine %C, %H and %N. Atomic absorption spectroscopy (AAS) was used to analyze of %metal in $Zn(OAc)_2$(tetraen) complex. The calculated results were different from experimental results (Table 4.3).

Table 4.3 Analytical characteristics of $Zn(OAc)_2$(tetraen) complex

Complex	Elements determined	Experimental (%)	Calculated (%)
$Zn(OAc)_2$(tetraen)	%Zn	14.75	17.50
($ZnC_{12}O_4H_{29}N_5$)	%C	41.96	38.64
	%H	7.94	7.84
	%N	14.64	18.80

4.2.2.4 Mass Spectrometry (MS) of $Zn(OAc)_2$(tetraen) Complex

The molecular ion peak corresponding to $[^{64}Zn(OAc)_2(tetraen).H_2O+H]^+$, $[^{66}Zn(OAc)_2(tetraen).H_2O+H]^+$ and $[^{64}Zn(OAc)_2(tetraen).3H_2O+H]^+$ appear as the protonated form at *m/z* of 390.32, 391.33 and 426.45, respectively (Table 4.4 and Figure 4.6). It was indicated that the complex of $Zn(OAc)_2$(tetraen) was formed.

Table 4.4 MS data of $Zn(OAc)_2$(tetraen) complex

Molecular ion	Found	Calculated
$[^{64}Zn(OAc)_2(tetraen).H_2O+H]^+$	390.32	390.17
$[^{66}Zn(OAc)_2(tetraen).H_2O+H]^+$	391.33	391.68
$[^{64}Zn(OAc)_2(tetraen).3H_2O+H]^+$	426.45	426.20

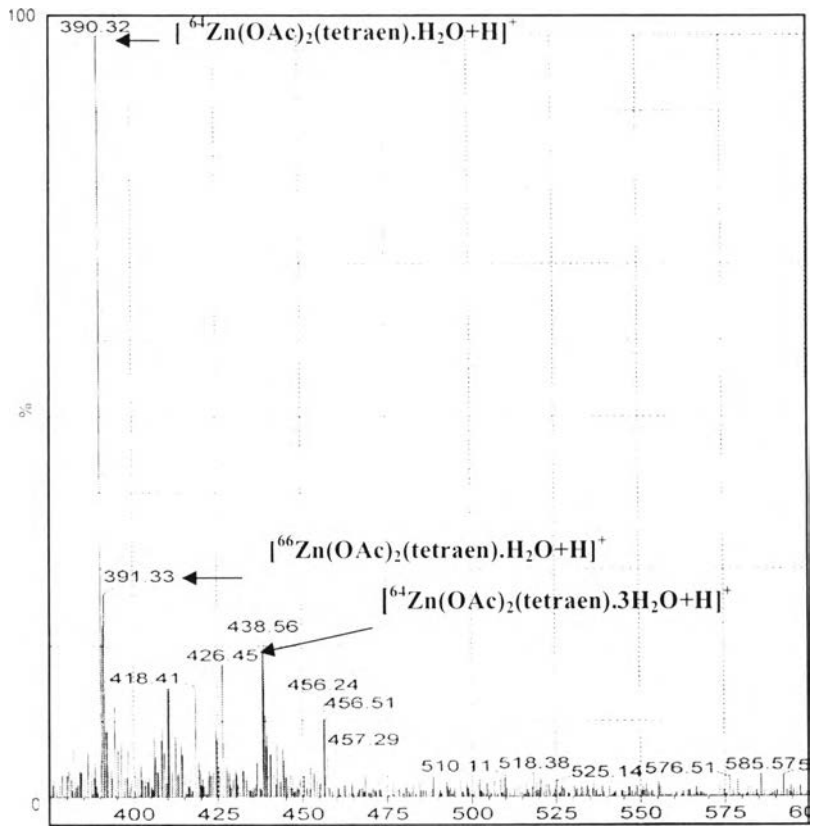

Figure 4.6 Mass spectrum of $Zn(OAc)_2$(tetraen) complex

4.2.3 Characterization of Mixed Metal-Amine Complex

4.2.3.1 IR Spectroscopy of $CuOAc)_2$(tetraen):$Zn(OAc)_2$(tetraen) Complex

IR spectrum of $Cu(OAc)_2$(tetraen) showed the following characteristic peaks at 3137-3251 cm^{-1} (N-H stretching), 2930 cm^{-1} (C-H stretching), 1557 (asymmetric C=O), 1392 cm^{-1} (symmetric C=O), 1334 cm^{-1} (C-N stretching) and 1007 cm^{-1} (C-O stretching). IR spectrum of $Zn(OAc)_2$(tetraen) showed characteristic peaks at 3163-3289 cm^{-1} (N-H stretching), 2927 cm^{-1} (C-H stretching), 1562 cm^{-1}(asymmetric C=O), 1388 cm^{-1} (symmetric C=O), 1331 cm^{-1} (C-N stretching) and 1003 cm^{-1} (C-O stretching).

N-H stretching, C-H stretching and C-N stretching of $Cu(OAc)_2$(tetraen):$Zn(OAc)_2$(tetraen) were observed at 3150-3240 cm^{-1}, 2928 cm^{-1} and 1332 cm^{-1}, respectively. They shifted from N-H stretching, C-H stretching and C-N stretching of tetraen, which appeared at 3184-3354 cm^{-1}, 2936 cm^{-1} and 1323 cm^{-1}, respectively. The C=O stretching of carbonyl group in $Cu(OAc)_2$(tetraen):$Zn(OAc)_2$(tetraen) appeared at 1558 cm^{-1} (asymmetric C=O) and 1390 cm^{-1} (symmetric C=O), which were different from those of $Cu(OAc)_2$ and $Zn(OAc)_2$ normally appear at 1589 cm^{-1} and 1549 cm^{-1} (asymmetric C=O), respectively, and 1416 cm^{-1} and 1443 cm^{-1} (symmetric C=O), respectively. The C-O stretching of $Cu(OAc)_2$(tetraen):$Zn(OAc)_2$(tetraen) was observed at 1008 cm^{-1} which shifted from that of $Cu(OAc)_2$ and $Zn(OAc)_2$ at 1032 cm^{-1} and 1017 cm^{-1}, respectively. It was indicated that the IR peaks of $Cu(OAc)_2$(tetraen):$Zn(OAc)_2$(tetraen) shifted from those $Cu(OAc)_2$ and $Zn(OAc)_2$ which confirmed that the complex was formed (Figure 4.7).

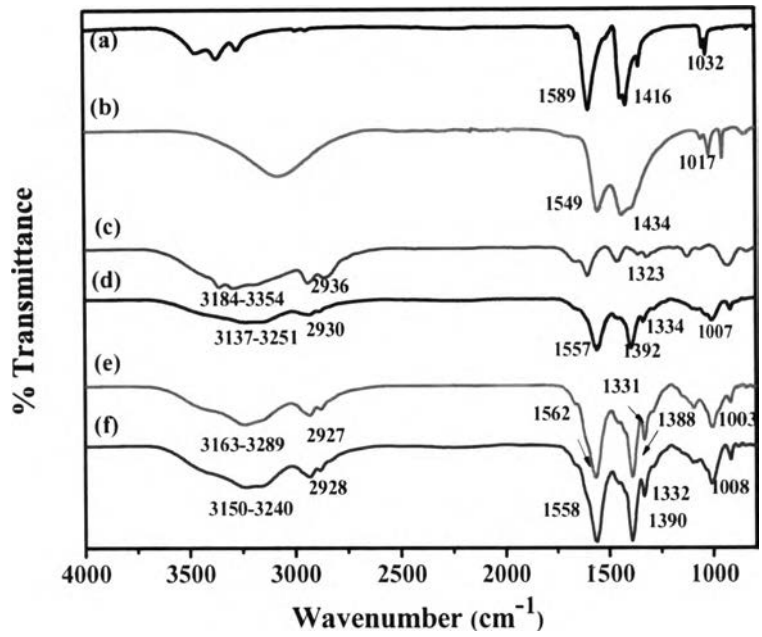

Figure 4.7 IR spectra of (a) $Cu(OAc)_2$; (b) $Zn(OAc)_2$; (c) tetraen; (d) $Cu(OAc)_2$ (tetraen); (e) $Zn(OAc)_2$(tetraen); (f) $Cu(OAc)_2$(tetraen):$Zn(OAc)_2$(tetraen)

4.2.3.2 UV-Visible Spectroscopy of $Cu(OAc)_2$(tetraen) :$Zn(OAc)_2$(tetraen) Complex

UV-visible spectra of $Cu(OAc)_2$ and $Zn(OAc)_2$ showed the absorption at 244 and 201 nm, respectively. UV-visible spectra of $Cu(OAc)_2$(tetraen):$Zn(OAc)_2$(tetraen) and $Cu(OAc)_2$(tetraen):$Zn(OAc)_2$(tetraen)-W synthesized in acetone and water, respectively, were compared. Both $Cu(OAc)_2$(tetraen):$Zn(OAc)_2$(tetraen) and $Cu(OAc)_2$(tetraen):$Zn(OAc)_2$(tetraen)-W gave the same absorption at 263 nm. It was indicated that $Cu(OAc)_2$(tetraen):$Zn(OAc)_2$(tetraen) could be obtained by using acetone and water in the synthesis because their UV peaks shifted from typical maximum absorption of $Cu(OAc)_2$ and $Zn(OAc)_2$. Moreover, UV-visible spectra of $Cu(OAc)_2$(tetraen) and $Cu(OAc)_2$(tetraen)-W showed at the same absorption at 264 nm. UV-visible spectra of $Zn(OAc)_2$(tetraen) and $Zn(OAc)_2$(tetraen)-W showed at the same absorption at 203 nm (Figure 4.8).

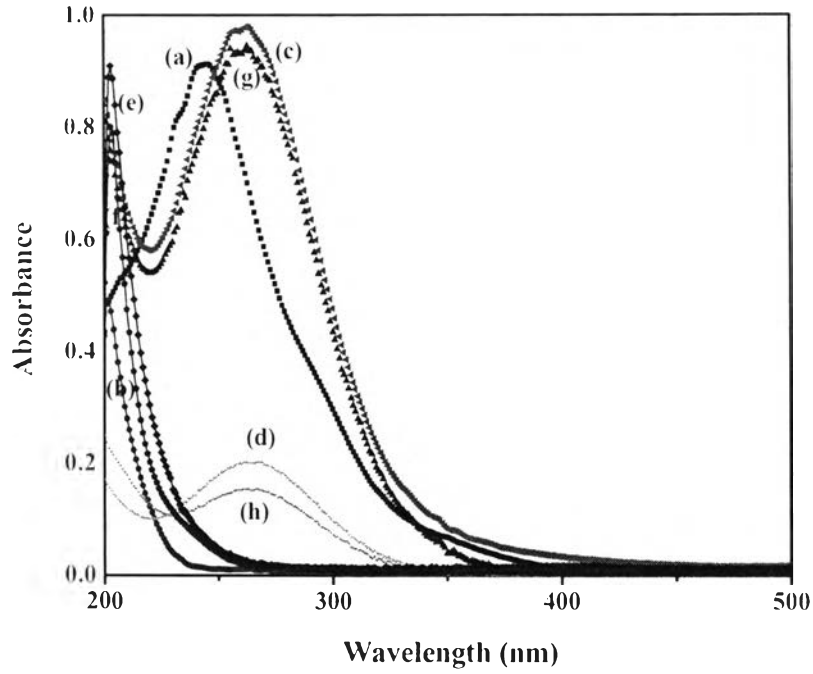

Figure 4.8 UV spectra of (a) $Cu(OAc)_2$; (b) $Zn(OAc)_2$; (c) $Cu(OAc)_2$(tetraen) (d) $Cu(OAc)_2$(tetraen)-W; (e) $Zn(OAc)_2$(tetraen); (f) $Zn(OAc)_2$(tetraen)-W; (g) $Cu(OAc)_2$(tetraen):$Zn(OAc)_2$(tetraen) ; (h) $Cu(OAc)_2$(tetraen) :$Zn(OAc)_2$(tetraen)-W

4.2.3.3 Analytical Characteristics of $CuOAc)_2$(tetraen): $Zn(OAc)_2$(tetraen) Complex

Elemental analysis (EA) was used to determine %C, %H and %N. Atomic absorption spectroscopy (AAS) was used to analyze of %metal in $Cu(OAc)_2$(tetraen):$Zn(OAc)_2$(tetraen) complex. The calculated results were different from experimental results (Table 4.5).

Table 4.5 Analytical characteristics of $Cu(OAc)_2$(tetraen):$Zn(OAc)_2$(tetraen) complex

Complex	Elements determined	Experimental (%)	Calculated (%)
$Cu(OAc)_2$(tetraen):$Zn(OAc)_2$(tetraen)	%Cu	8.0	8.54
($CuZnC_{24}O_8H_{58}N_{10}$)	%Zn	7.0	8.79
	%C	39.66	38.74
	%H	7.93	7.86
	%N	15.60	18.85

4.2.3.4 Mass Spectrometry (MS) of $Cu(OAc)_2$(tetraen): $Zn(OAc)_2$(tetraen) Complex

The molecular ion peak corresponding to $[^{63}Cu(OAc)_2(tetraen)+H]^+$ and $[^{65}Cu(OAc)_2(tetraen).H_2O+H]^+$ appear as the protonated form at *m/z* of 370.28 and 391.47, respectively. The molecular ion peak corresponding to $[^{64}Zn(OAc)_2(tetraen).H_2O+H]^+$, $[^{66}Zn(OAc)_2(tetraen).H_2O+H]^+$ and $[^{64}Zn(OAc)_2(tetraen).3H_2O+H]^+$ appear as the protonated form at m/z of 390.36, 391.25 and 426.45, respectively (Table 4.6 and Figure 4.9). It was indicated that complexes of $Cu(OAc)_2$(tetraen) and $Zn(OAc)_2$(tetraen) were formed.

Table 4.6 MS data of $Cu(OAc)_2$(tetraen):$Zn(OAc)_2$(tetraen) complex

Molecular ion	Found	Calculated
$[^{63}Cu(OAc)_2(tetraen)+H]^+$	370.28	370.96
$[^{64}Zn(OAc)_2(tetraen).H_2O+H]^+$	390.36	390.17
$[^{66}Zn(OAc)_2(tetraen).H_2O+H]^+$	391.25	391.68
$[^{65}Cu(OAc)_2(tetraen).H_2O+H]^+$	391.47	391.17
$[^{64}Zn(OAc)_2(tetraen).3H_2O+H]^+$	426.45	426.20

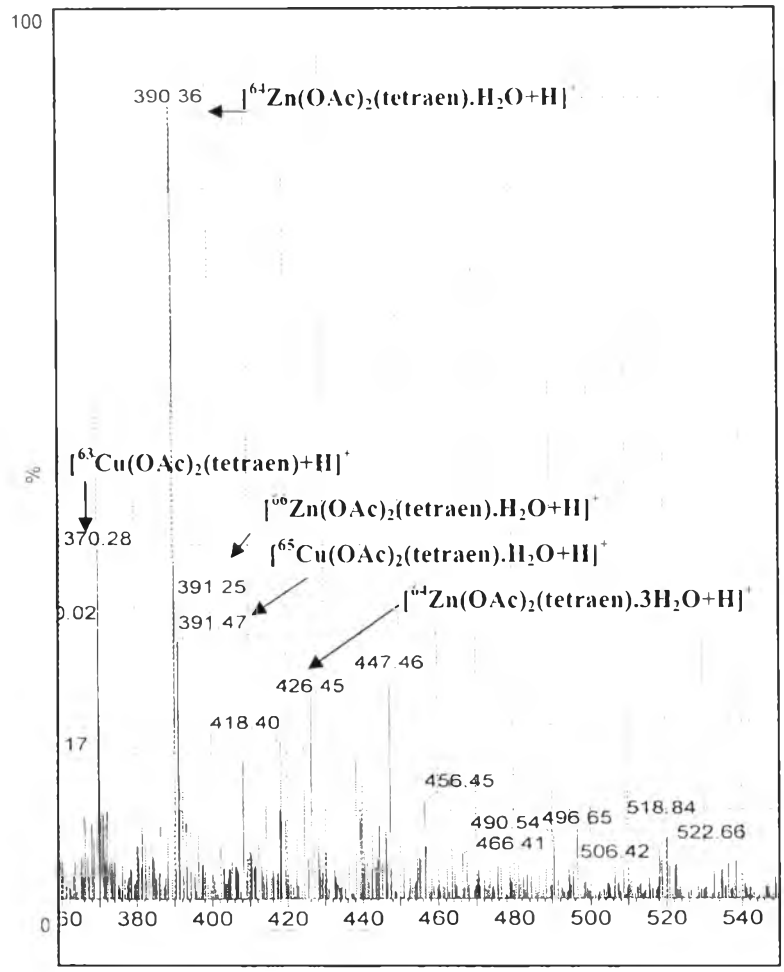

Figure 4.9 Mass spectrum of $Cu(OAc)_2$(tetraen):$Zn(OAc)_2$(tetraen) complex

4.3 Preparation of Rigid Polyurethane Foams (RPUR foams)

4.3.1 Effect of Metal (II) Acetate:Amine Ratios

RPUR foams were prepared from metal-amine and mixed metal-amine complexes with variable metal (II) acetate:amine [$M(OAc)_2$:tetraen] mole ratios of 1:2, 1:1 and 1:0.5. Metal complexes were synthesized in acetone and water. It was found that reaction times and density of RPUR foams synthesized in acetone corresponded with those synthesized in water. Foams catalyzed by metal complexes prepared at the $M(OAc)_2$:tetraen ratio of 1:0.5 had good catalytic activity. However, it was difficult to dissolve these metal complexes in polyol. Metal complexes prepared at the $M(OAc)_2$:tetraen ratio of 1:2 had long reaction times and gave too high density. It was

clear that RPUR foams catalyzed by Ni(tetraen) showed longer tack free time than ten minutes. The complexes prepared from $M(OAc)_2$:tetraen ratio of 1:1 showed the best reaction times and density for preparing RPUR foams. Therefore, the complexes prepared from $M(OAc)_2$:tetraen ratio of 1:1 were used to prepare RPUR foams at NCO index of 100 in order to study the effect of formulations content on their reaction times and density. The reaction times of RPUR foams catalyzed by mixed metal-amine complexes were as good as metal-amine complexes. The mixed metal-amine complexes could give the desired properties of RPUR foams. The formulations and reaction times of RPUR foams with variable $M(OAc)_2$:tetraen ratios are shown in Tables 4.7 and 4.8, respectively. Standard deviation (S.D.) of the data in Table 4.8 is shown in Table B3 (Appendix B).

Metal complexes could catalyze RPUR foams polymerization since the metal complexes acted as Lewis acid, primary coordinated to the oxygen atom of the NCO group and activated the electrophilic nature of carbon. The amine used its lone pair of electrons interacting with the proton source (polyol, water and amine) to form a complex and react with isocyanate [2, 6]. $M(OAc)_2$ or tetraen could be used to prepare RPUR foams but they gave long reaction time and undesirable foam properties. Therefore, metal-amine complexes were synthesized in order to obtained suitable reaction times and external appearance of RPUR foams. The mole ratio of metal (II) acetate and tetraen was investigated because the steric hindrance of tetraen had the effect on catalytic activity [3]. The proposed structures of metal complexes with variation of $M(OAc)_2$:tetraen ratios are shown in Figure 4.10

Table 4.7 Formulations of RPUR foams

Formulations	pbw
$M(OAc)_2$:tetraen	1:2, 1:1, 1:0.5
Polyol	100.0
Surfactant	2.5
Blowing agent	3.0
Catalyst	1.2
PMDI	152.6
NCO index	100

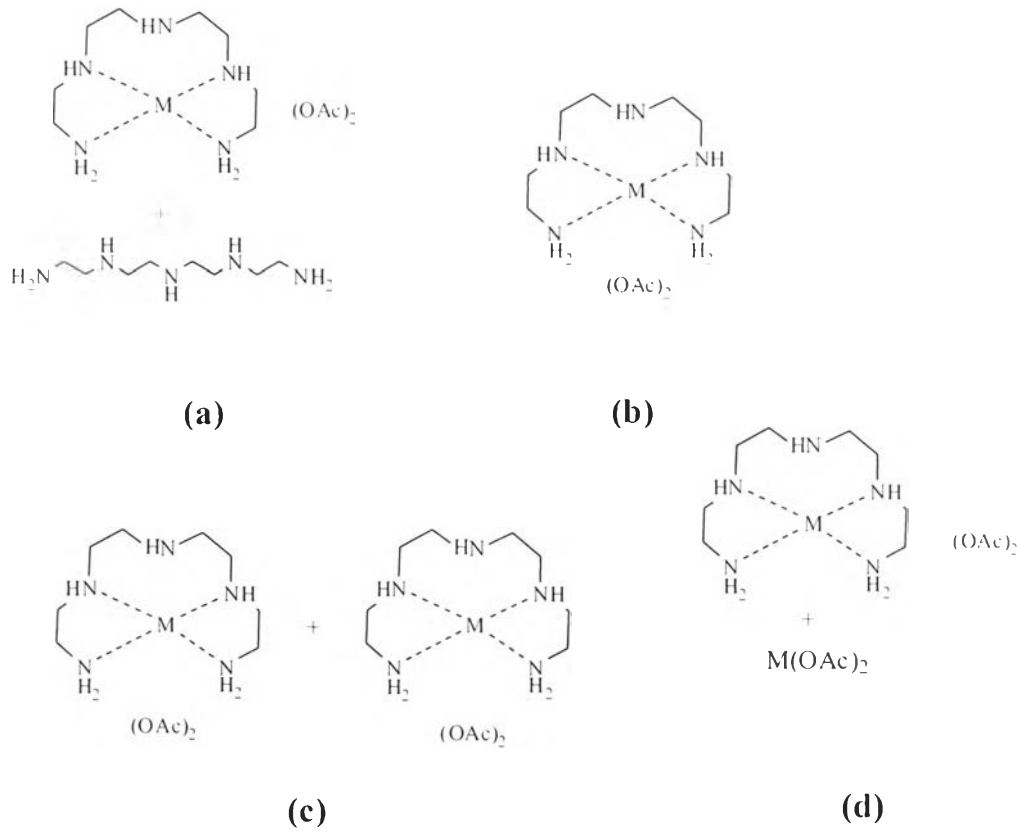

Figure 4.10 Proposed structure of metal complexes and mixed metal complexes with variable $M(OAc)_2$:tetraen ratios (a) 1:2; (b) 1:1; (c) 1:1; (d) 1:0.5

Table 4.8 Reaction times of RPUR foams prepared at the NCO index of 100

Catalysts	$M(OAc)_2$:tetraen	Cream time (min)	Gel time (min)	Rise time (min)	Tack free time (min)	Density (kg/m^3)	Volume (V/8)
Cu(tetraen)	1:2	0:38	1:00	3:20	3:42	41.5	6.5
Zn(tetraen)	1:2	0:37	1:08	5:12	5:30	36.7	7.0
Ni(tetraen)	1:2	0:37	1:35	11:30	14:12	47.8	5.5
Co(tetraen)	1:2	0:39	1:30	7:30	8:40	38.4	7.0
Mn(tetraen)	1:2	0:37	1:20	8:22	9:28	44.9	6.0
Cu(tetraen): Zn(tetraen)	1:2	0:38	1:02	3:58	3:42	40.0	7.0
Cu(tetraen): Ni(tetraen)	1:2	0:38	1:24	7:05	7:05	46.8	6.0
Cu(tetraen):Co(tetraen)	1:2	0:40	1:07	4:20	4:10	42.0	6.0
Cu(tetraen):Mn(tetraen)	1:2	0:36	1:25	6:12	6:40	46.5	6.5
Cu(tetraen)-W	1:2	0:36	0:54	3:05	3:22	40.0	6.8
Zn(tetraen)-W	1:2	0:35	1:00	5:00	5:14	37.0	7.0
Cu(tetraen): Zn(tetraen)-W	1:2	0:36	0:55	3:30	3:12	39.7	7.0
Cu(tetraen)	1:1	0:35	0:48	2:25	2:12	38.4	7.0
Zn(tetraen)	1:1	0:33	1:05	4:40	4:55	35.0	8.0
Cu(tetraen): Zn(tetraen)	1:1	0:36	0:56	3:06	2:43	37.0	7.5
Cu(tetraen)-W	1:1	0:32	0:46	2:10	2:00	38.2	7.0
Zn(tetraen)-W	1:1	0:32	0:56	4:30	4:45	35.5	8.0
Cu(tetraen): Zn(tetraen)-W	1:1	0:34	0:52	3:12	2:35	37.4	7.5
Cu(tetraen)	1:0.5	0:34	0:50	2:00	2:10	42.7	6.5
Cu(tetraen): Zn(tetraen)	1:0.5	0:36	0:46	2:20	2:05	37.5	7.5
Cu(tetraen)-W	1:0.5	0:36	0:45	2:30	2:10	38.6	7.0
Cu(tetraen): Zn(tetraen)-W	1:0.5	0:35	0:56	2:40	2:15	38.0	7.5

4.3.2 Effect of Catalysts on Rigid Polyurethane Foams (RPUR Foams) Properties

Catalysts play an important role in accelerating the blowing and gelling reactions. Catalyst content was adjusted for the suitable formulations. The optimum catalyst content had effect on reaction times, density and appearance of RPUR foams. RPUR foams could not be obtained with too small catalyst amount. On the other hand, the excess of catalyst content resulted in waste. The effect of catalyst content on reaction times, volume and density were investigated and shown in Table 4.9. S.D. of the data in Table 4.9 is shown in Table B4 (Appendix B).

Table 4.9 Effect of catalyst content on reaction times, density and volume of RPUR foams prepared at the NCO index of 100

Catalysts	Catalyst Content (pbw)	Cream time (min)	Gel time (min)	Rise time (min)	Tack free time (min)	Density (kg/m^3)	Volume (V/8)
DMCHA	0.25	0:30	1:02	6:40	8:50	39.4	6.25
Cu(tetraen)	0.25	0:37	1:26	5:33	5:52	48.0	5.50
Zn(tetraen)	0.25	0:38	1:50	7:55	8:20	44.4	5.75
Cu(tetraen): Zn(tetraen)	0.25	0:37	1:33	6:44	7:04	46.5	5.75
Cu(tetraen)-W	0.25	0:35	1:20	5:00	5:25	47.2	5.50
Zn(tetraen)-W	0.25	0:34	1:46	7:22	7:55	43.9	5.75
Cu(tetraen): Zn(tetraen)-W	0.25	0:35	1:32	6:18	6:40	45.6	5.75
DMCHA	0.50	0:28	0:41	3:10	4:28	37.0	7.00
Cu(tetraen)	0.50	0:35	1:09	3:52	3:40	43.0	6.25
Zn(tetraen)	0.50	0:33	1:32	5:44	6:00	40.5	6.50
Cu(tetraen): Zn(tetraen)	0.50	0:35	1:16	4:40	4:26	41.8	6.50
Cu(tetraen)-W	0.50	0:33	1:05	3:36	3:20	42.7	6.25
Zn(tetraen)-W	0.50	0:30	1:30	5:20	5:38	40.1	6.50
Cu(tetraen): Zn(tetraen)-W	0.50	0:33	1:13	4:21	4:00	41.5	6.50
DMCHA	1.00	0:20	0:25	1:58	2:25	35.2	7.25
Cu(tetraen)	1.00	0:33	0:46	2:42	2:30	38.0	7.25
Zn(tetraen)	1.00	0:30	1:02	4:08	4:20	36.0	7.50
Cu(tetraen): Zn(tetraen)	1.00	0:32	0:54	3:30	3:15	37.1	7:50
Cu(tetraen)-W	1.00	0:29	0:42	2:22	2:08	37.7	7.25
Zn(tetraen)-W	1.00	0:29	0:56	3:30	3:48	35.8	7.50
Cu(tetraen): Zn(tetraen)-W	1.00	0:32	0:48	3:08	2:52	36.6	7.50

4.3.2.1 Effect of Catalyst Content on Reaction Time of RPUR Foams

Reaction times of RPUR foams prepared by Cu(tetraen), Zn(tetraen) and Cu(tetraen):Zn(tetraen) synthesized in acetone and water are shown in Figures 4.11 and 4.12, respectively. The results indicated clearly that the rate of foaming reaction increased with the increase of catalyst content. Conspicuously, the increasing of Cu(tetraen) content promoted gelling reaction, which was confirmed by the faster gel time and tack free time. Moreover, the increasing of Zn(tetraen) content accelerated foams rising which resulted in higher volume of RPUR foams (Table 4.9). Therefore, Zn(tetraen) could promote blowing reaction. RPUR foams prepared by mixed metal-amine complex, Cu(tetraen):Zn(tetraen) had faster gel time and tack free time than those prepared by Zn(tetraen). Since Cu(tetraen) in Cu(tetraen):Zn(tetraen) accelerated gelling reaction. Cu(tetraen):Zn(tetraen) gave higher foam volume than Cu(tetraen) because of Zn(tetraen) in Cu(tetraen):Zn(tetraen). M(tetraen)-W gave slightly faster tack free time than M(tetraen) since M(tetraen)-W could be easily formed in water, which also served as a blowing agent. The complex preparation in water consumes less time than preparation in acetone. The catalytic activities of metal complexes and commercial catalyst (DMCHA) were compared. The results indicated that Cu(tetraen) accelerated RPUR foam formation faster than DMCHA. The increasing of DMCHA content promoted the blowing and gelling reactions, which were confirmed by the faster cream time and tack free time, respectively.

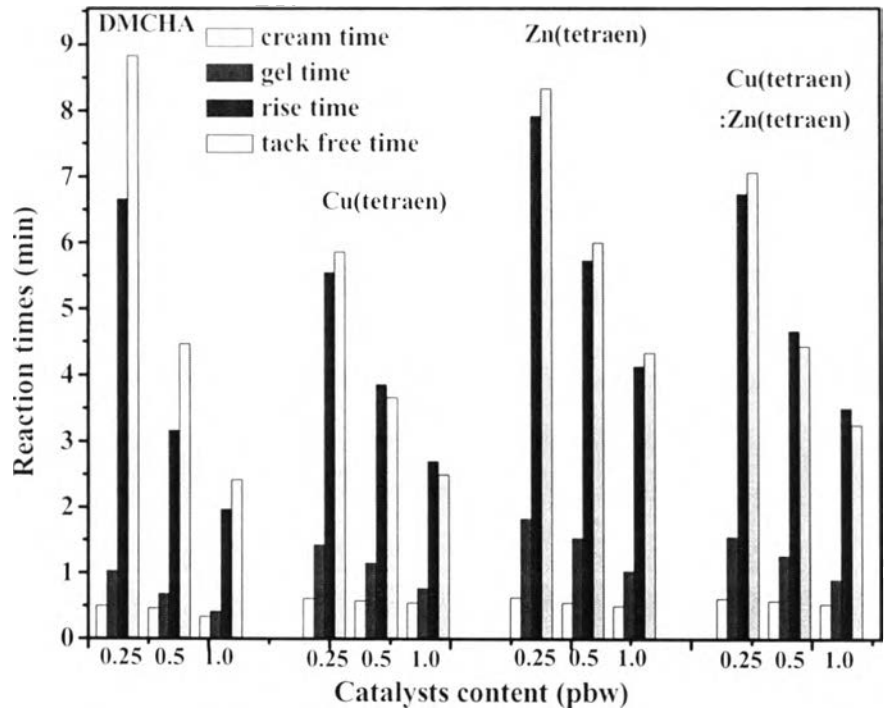

Figure 4.11 The effect of catalyst content on reaction times of RPUR foams prepared at the NCO index of 100 and catalyzed by DMCHA; Cu(tetraen); Zn(tetraen); Cu(tetraen):Zn(tetraen)

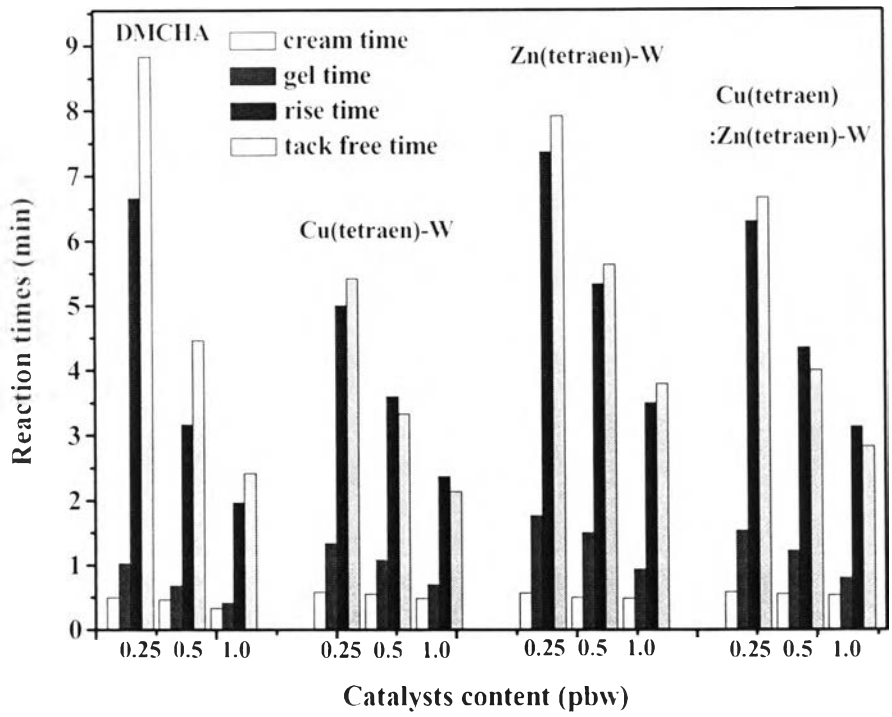

Figure 4.12 The effect of catalyst content on reaction times of RPUR foams prepared at the NCO index of 100 and catalyzed by DMCHA; Cu(tetraen)-W; Zn(tetraen)-W; Cu(tetraen):Zn(tetraen)-W

4.3.2.2 Effect of Catalyst Content on Density of RPUR Foams

The catalyst content had an influence on density of RPUR foams. In Figures 4.13 and 4.14, all density of RPUR foams decreased with increasing of catalyst content due to promotion of the blowing reaction. Conspicuously, the foams catalyzed by Zn(tetraen) showed less density than those catalyzed by Cu(tetraen). Therefore, Zn(tetraen) was blowing catalyst which confirmed by cream time, foam volume and density. The blowing gas was increasing generated and conduced to low density [1]. RPUR foams catalyzed by M(tetraen) and M(tetraen)-W had the same density. They gave higher foam density than DMCHA. DMCHA at catalyst content 0.10 pbw had low density due to DMCHA was blowing catalyst [5]. In addition, bubble could be generated by mixing and trapped during foam formation. The bubble resulted in low density RPUR foams. The catalyst content at 0.50 pbw gave the optimum foam density, which was in the range of 40.1-43.0 kg/m^3 at the NCO index of 100. Therefore, the

catalyst content at 0.50 pbw was used to study reaction times and properties of RPUR foams.

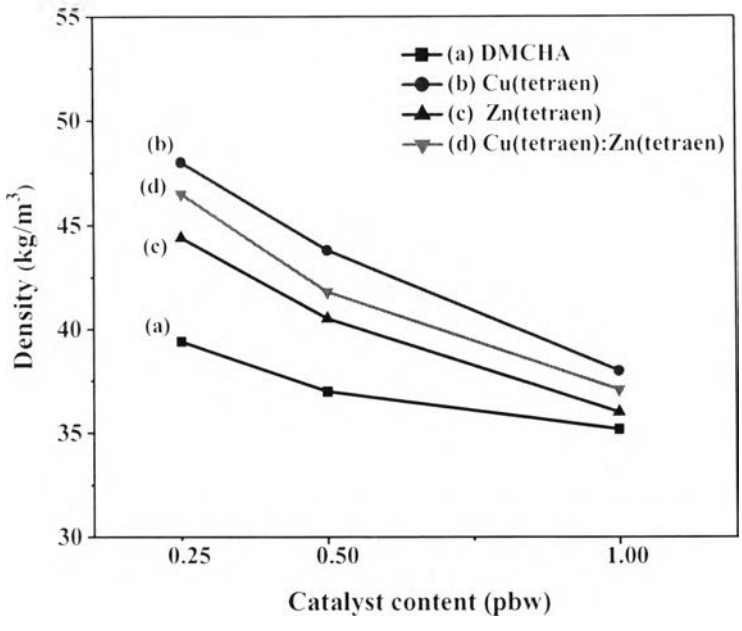

Figure 4.13 The effect of catalyst content on density of RPUR foams prepared at the NCO index of 100 and catalyzed by (a) DMCHA; (b) Cu(tetraen); (c) Zn(tetraen); (d) Cu(tetraen):Zn(tetraen)

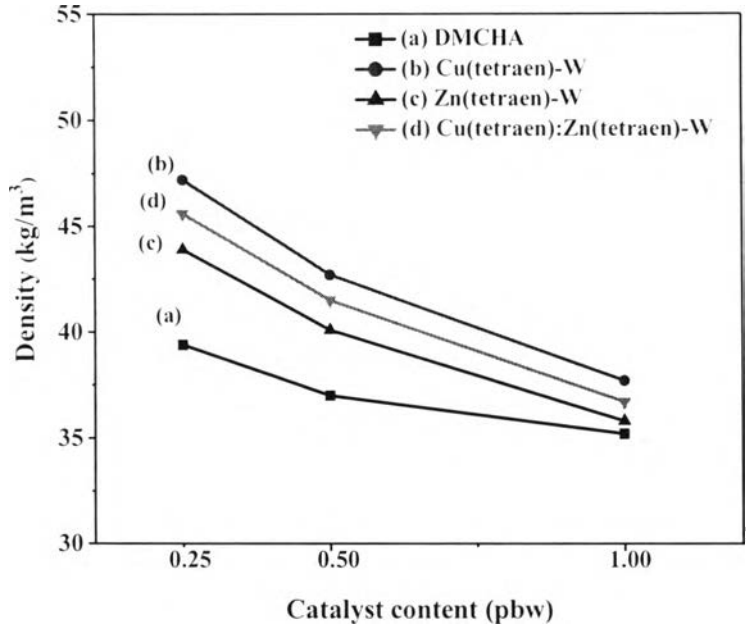

Figure 4.14 The effect of catalyst content on density of RPUR foams prepared at the NCO index of 100 and catalyzed by (a) DMCHA; (b) Cu(tetraen)-W; (c) Zn(tetraen)-W; (d) Cu(tetraen):Zn(tetraen)-W

4.3.3 Effect of Blowing Agent Content on Rigid Polyurethane Foams (RPUR Foams)

The effect of blowing agent (water) content on density of RPUR foams synthesized from M(tetraen) and M(tetraen)-W are shown in Figures 4.15 and 4.16, respectively. Reaction times and their S.D. are shown in Table B7-B13 (Appendix B). It was found that density of the RPUR foams decreased with increasing of blowing agent content from 0 to 4.0 pbw. Blowing reaction resulted from the reaction of water with isocyanates to produce carbon dioxide gas and amine. Therefore, the increase of water content produced more gas bubbles [10]. Moreover, RPUR foams synthesized from M(tetraen) and M(tetraen)-W showed similar density. RPUR foams catalyzed by DMCHA had the lowest density. The density of RPUR foams obtained from 2 pbw of blowing agent was in the range of 40-50 kg/m^3, which was the suitable density for foam applications. When the blowing agent was increased to 4 pbw, the density of RPUR

foams was slightly changed due to the excess isocyanate in the formulation, which resulted in the brittle foams.

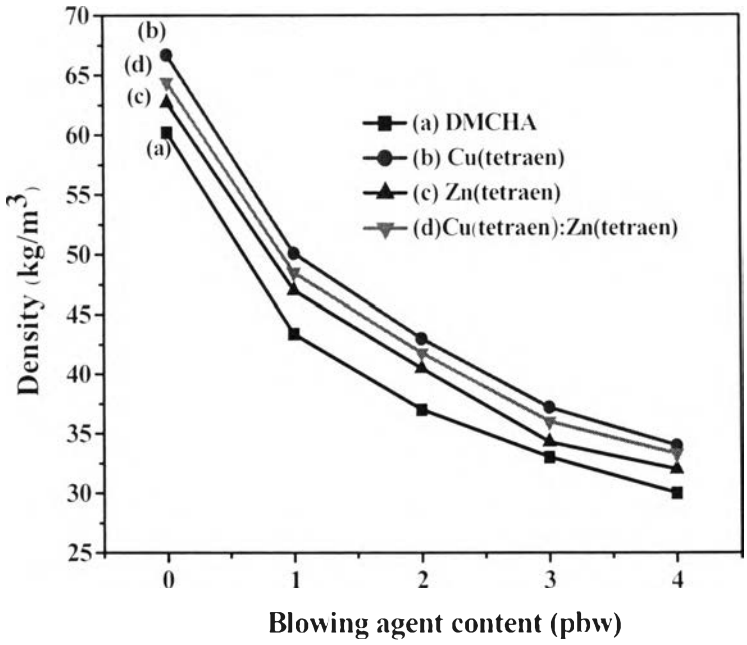

Figure 4.15 The effect of blowing agent content on density of RPUR foams prepared at the NCO index of 100 and catalyzed by (a) DMCHA; (b) Cu(tetraen); (c) Zn(tetraen); (d) Cu(tetraen):Zn(tetraen)

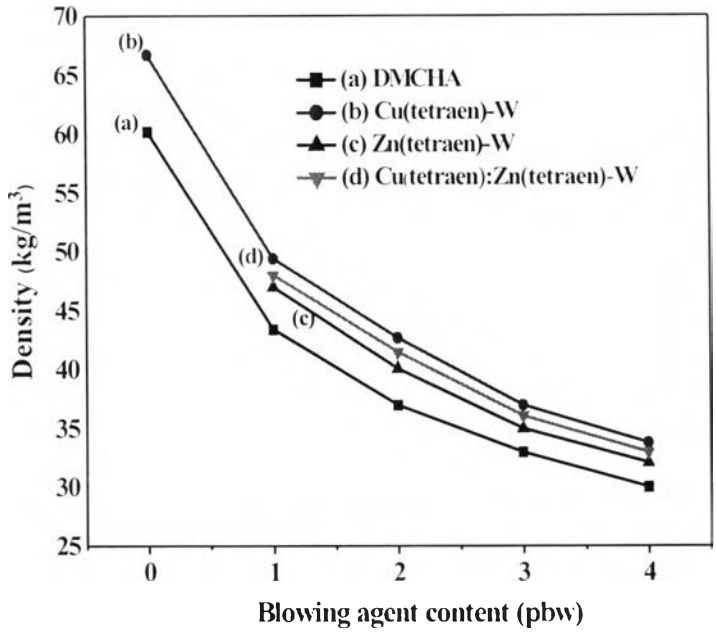

Figure 4.16 The effect of blowing agent content on density of RPUR foams prepared at the NCO index of 100 and catalyzed by (a) DMCHA; (b) Cu(tetraen)-W; (c) Zn(tetraen)-W; (d) Cu(tetraen):Zn(tetraen)-W

Therefore, the optimum blowing agent was 2 pbw. The suitable formulations are listed in Table 4.10 used for preparing and testing RPUR foams.

Table 4.10 The optimum formulations for preparing RPUR foams

Formulations	pbw
$M(OAc)_2$:tetraen	1:1
Polyol	100.0
Surfactant	2.5
Blowing agent	2.0
Catalyst	0.5
PMDI	131.6
NCO index	100

4.3.4 Effect of $M_1(OAc)_2$:$M_2(OAc)_2$ Ratios in Metal Complexes

Mixed metal complex of Cu(tetraen):Zn(tetraen) with variable $Cu(OAc)_2$:$Zn(OAc)_2$:tetraen ratios of 0.7:0.3:1, 0.5:0.5:1 and 0.3:0.7:1 were synthesized in acetone and water. It was found that the reaction times of RPUR foams decreased with increasing of $Cu(OAc)_2$ ratio which was confirmed by the faster gel time and tack free time. Cu(tetraen):Zn(tetraen) and Cu(tetraen):Zn(tetraen)-W showed similar trend. Reaction profiles of RPUR foams with variable $Cu(OAc)_2$:$Zn(OAc)_2$:tetraen ratios are shown in Table 4.11, Figures 4.17 and 4.18. S.D. of the data is shown in Table B5 (Appendix B).

Table 4.11 Effect of $M_1(OAc)_2$:$M_2(OAc)_2$ ratios on reaction time, density and volume of RPUF foams prepared at the NCO index of 100

Catalysts	$M_1(OAc)_2$: $M_2(OAc)_2$: tetraen	Cream time (min)	Gel time (min)	Rise time (min)	Tack free time (min)	Density (kg/m^3)	Volume (V/8)
Cu(tetraen):Zn(tetraen)	0.7:0.3:1	0:35	1:10	4:10	3:56	42.3	6.50
Cu(tetraen):Zn(tetraen)	0.5:0.5:1	0:35	1:16	4:40	4:26	41.8	6.50
Cu(tetraen):Zn(tetraen)	0.3:0.7:1	0:34	1:21	5:10	4:45	40.2	6.75
Cu(tetraen):Zn(tetraen)-W	0.7:0.3:1	0:35	1:05	4:02	3:50	42.5	6.50
Cu(tetraen):Zn(tetraen)-W	0.5:0.5:1	0:33	1:13	4:21	4:00	41.5	6.50
Cu(tetraen):Zn(tetraen)-W	0.3:0.7:1	0:33	1:20	4:57	4:36	40.3	6.75

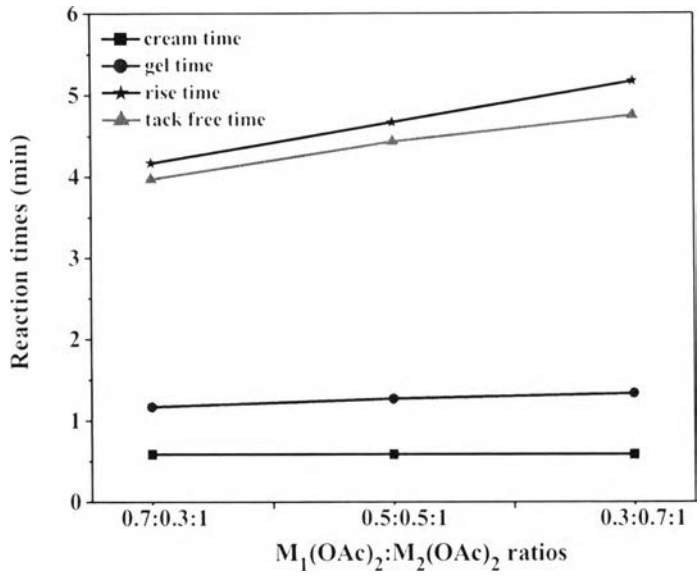

Figure 4.17 Reaction times of RPUR foams prepared at the NCO index of 100 and catalyzed by Cu(tetraen):Zn(tetraen) with different $Cu(OAc)_2$:$Zn(OAc)_2$ ratios

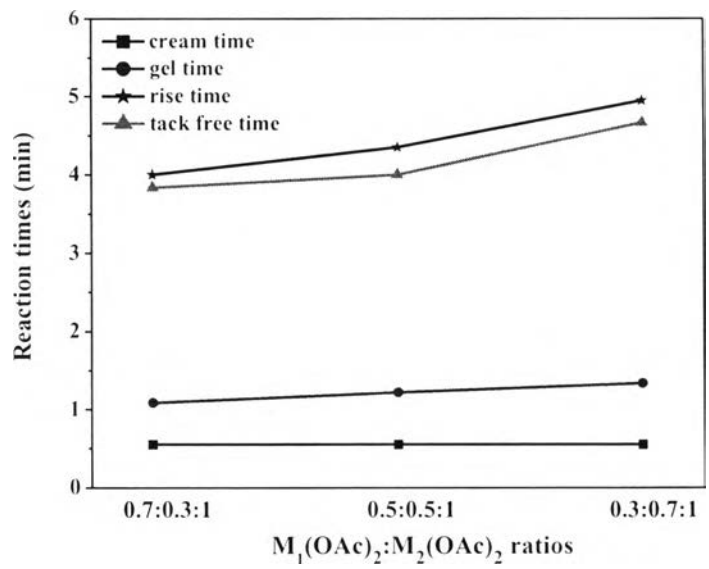

Figure 4.18 Reaction times of RPUR foams prepared at the NCO index of 100 and catalyzed by Cu(tetraen):Zn(tetraen)-W with different $Cu(OAc)_2$:$Zn(OAc)_2$ ratios

4.3.5 Effect of Mixed Amines [Ethylenediamine (en) and Triethylenetetramine (trien)] in Metal Complexes

Ethylenediamine (en) and triethylenetetramine (trien) were used as amine mixture with tetraen in the preparation of metal complexes. The ratio of $M(OAc)_2$:tetraen:en and $M(OAc)_2$:tetraen:trien was 1:0.5:0.5. The reaction times of RPUR foams catalyzed by metal complexes prepared from mixed amines are shown in Table 4.12, Figures 4.19 and 4.20. S.D. of the data is shown in Table B6 (Appendix B). The results indicated that en and trien promoted gelling reaction which was confirmed by faster gel time and tack free time. The data corresponded with Pengjam [27], where RPUR foams were prepared using $M(en)_2$ and M(trien) as catalysts.

Table 4.12 Effect of mixed amines (en and trien) in metal complexes on reaction time, density and volume of RPUF foams prepared at the NCO index of 100

Catalysts	Cream time (min)	Gel time (min)	Rise time (min)	Tack free time (min)	Density (kg/m^3)	Volume (V/8)
Cu(tetraen)	0:35	1:09	3:52	3:40	43.0	6.25
Zn(tetraen)	0:33	1:32	5:44	6:00	40.5	6.50
Cu(tetraen):Zn(tetraen)	0:35	1:16	4:40	4:26	41.8	6.50
Cu(tetraen)(en)	0:30	0:55	3:42	3:25	43.3	6.25
Zn(tetraen)(en)	0:28	1:15	5:40	5:17	40.7	6.50
Cu(tetraen)(en):Zn(tetraen)(en)	0:30	1:08	4:22	4:00	42.0	6.50
Cu(tetraen)(trien)	0:30	1:05	3:45	3:30	43.5	6.25
Zn(tetraen)(trien)	0:30	1:14	5:35	5:20	40.2	6.50
Cu(tetraen)(trien):Zn(tetraen)(trien)	0:29	1:12	4:35	4:15	41.4	6.50

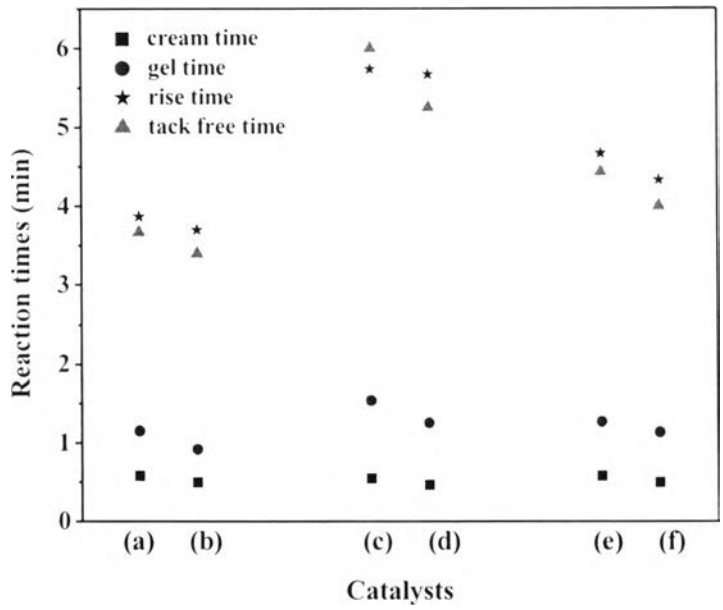

Figure 4.19 Reaction times of RPUR foams prepared at the NCO index of 100 and catalyzed by (a) Cu(tetraen); (b) Cu(tetraen)(en); (c) Zn(tetraen); (d) Zn(tetraen)(en); (e) Cu(tetraen):Zn(tetraen); (f) Cu(tetraen)(en): Zn(tetraen)(en)

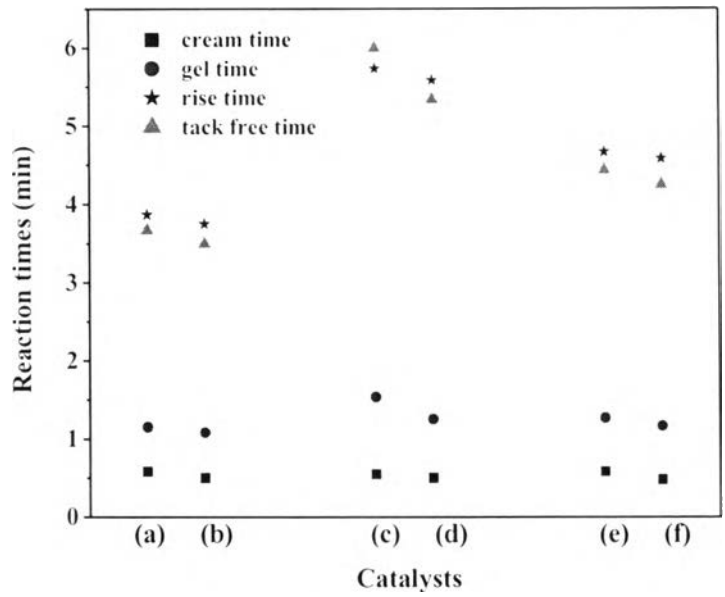

Figure 4.20 Reaction times of RPUR foams prepared at the NCO index of 100 and catalyzed by (a) Cu(tetraen); (b) Cu(tetraen)(trien); (c) Zn(tetraen); (d) Zn(tetraen)(trien); (e) Cu(tetraen):Zn(tetraen); (f) Cu(tetraen)(trien):Zn(tetraen)(trien)

4.3.6 Rise Profiles of Rigid Polyurethane Foams (RPUR Foams)

Table 4.13, Figures 4.21 and 4.22 show rise profiles of RPUR foams catalyzed by DMCHA, metal-amine and mixed metal-amine complexes. RPUR foams catalyzed by DMCHA had faster rise time than those catalyzed by metal complexes. DMCHA showed a short time at the initiate of the reaction. Rise profiles of RPUR foams catalyzed by M(tetraen) had similar trend to those catalyzed by M(tetraen)-W.

As shown in Figures 4.21 and 4.22, the maximum slope could be calculated for the maximum rise rate. RPUR foams prepared from DMCHA had higher maximum rise rate than those prepared from metal complexes. Figure 4.23 shows the maximum rise rate of RPUR foams catalyzed by DMCHA, M(tetraen) and M(tetraen)-W.

Table 4.13 Rise time at maximum rise height of RPUR foams prepared at the NCO index of 100

Catalysts	Rise time (s) at maximum rise height
DMCHA	190 (3:10)
Cu(tetraen)	232 (3:52)
Zn(tetraen)	344 (5:44)
Cu(tetraen):Zn(tetraen)	280 (4:40)
Cu(tetraen)-W	215 (3:36)
Zn(tetraen)-W	320 (5:20)
Cu(tetraen):Zn(tetraen)-W	261 (4:21)

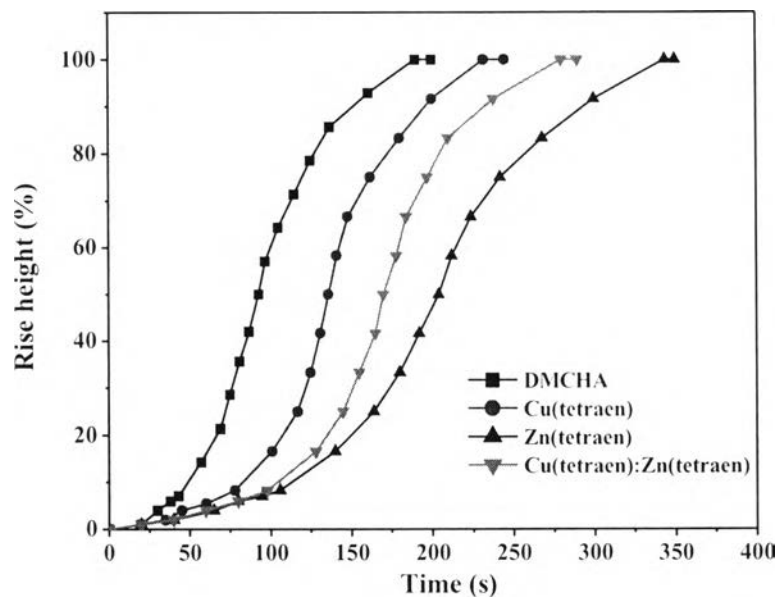

Figure 4.21 Rise profiles of RPUR foams catalyzed by DMCHA; Cu(tetraen); Zn(tetraen); Cu(tetraen):Zn(tetraen)

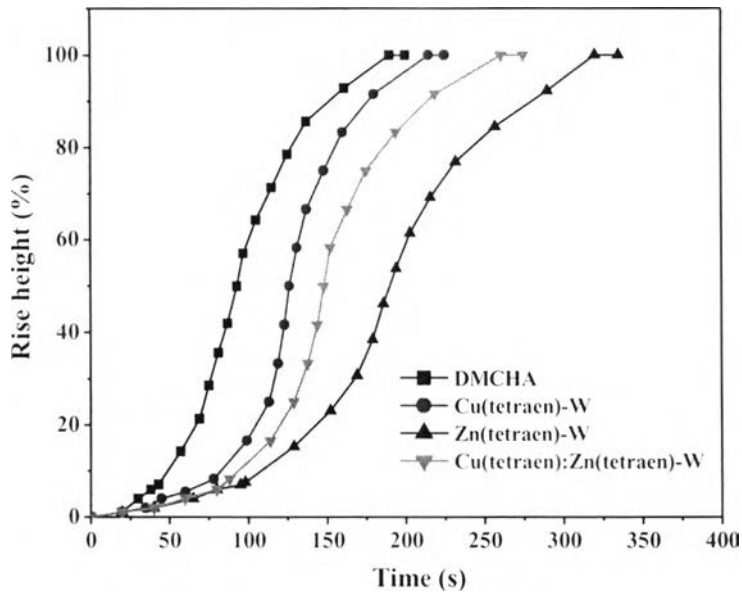

Figure 4.22 Rise profiles of RPUR foams catalyzed by DMCHA; Cu(tetraen)-W; Zn(tetraen)-W; Cu(tetraen):Zn(tetraen)-W

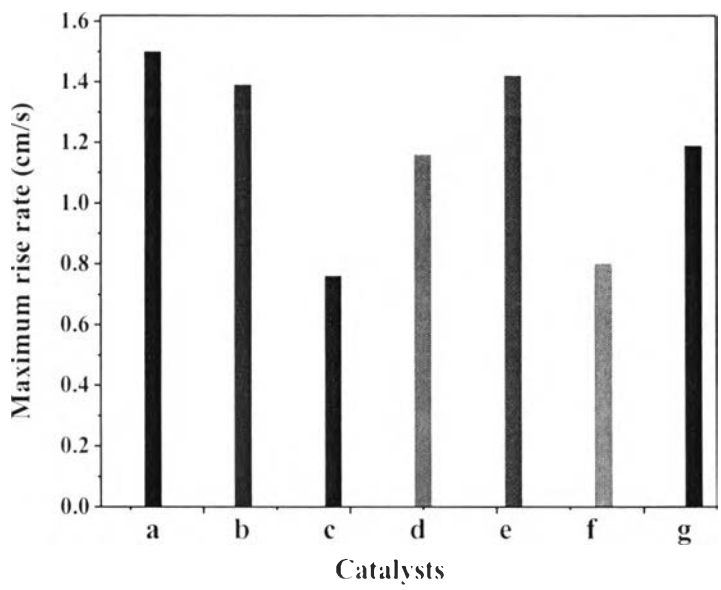

Figure 4.23 Maximum rise rates of RPUR foams prepared at the NCO index of 100 and catalyzed by (a) DMCHA; (b) Cu(tetraen); (c) Zn(tetraen); (d) Cu(tetraen):Zn(tetraen); (e) Cu(tetraen)-W; (f) Zn(tetraen)-W; (g) Cu(tetraen):Zn(tetraen)-W

4.3.7 Foaming Temperature

Figure 4.24 shows foaming temperature profiles of RPUR foams at the NCO index of 100. It was found that Cu(tetraen):Zn(tetraen) and Cu(tetraen):Zn(tetraen)-W showed the same temperature profiles. The foaming temperature gradually increased after the starting materials were mixed. The results indicated that RPUR foams polymerization reaction is exothermic reaction. The maximum core temperature (T_{max}) of RPUR foams is shown in Table 4.14. T_{max} increased with the increasing of NCO index. Since the excess amount of isocyanate in formulation could react with amine, the by product from the reaction of isocyanate and water, and generated disubstituted urea. This chemical reaction is also exothermic reaction increasing the foaming temperature. From Table 4.14, T_{max} of RPUR foams at the NCO indexes of 100 and 150 were in the range of 120 to 126 °C and 130 to 135 °C, respectively.

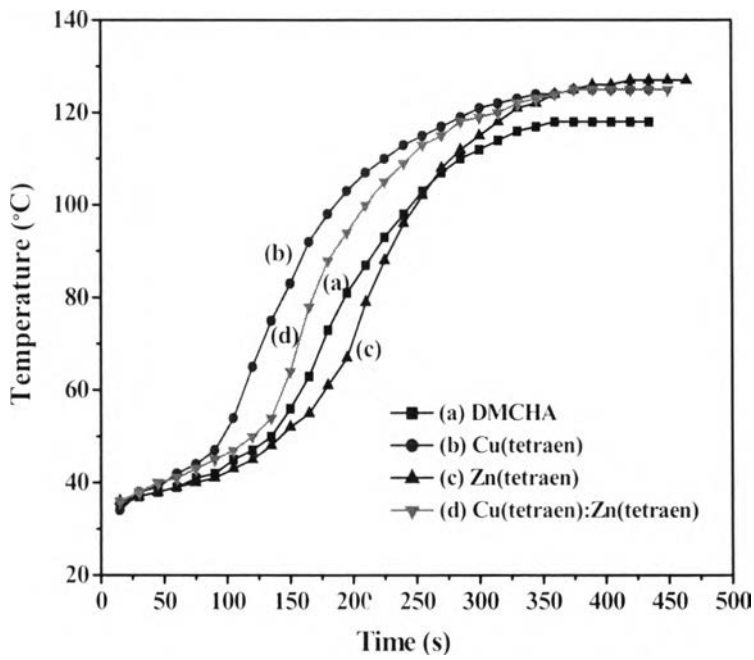

Figure 4.24 Temperature profiles of RPUR foams prepared at the NCO index of 100 and catalyzed by (a) DMCHA; (b) Cu(tetraen); (c) Zn(tetraen); (d) Cu(tetraen):Zn(tetraen)

Table 4.14 Maximum core temperature of RPUR foams prepared at the NCO indexes of 100-150 and catalyzed by different catalysts

Catalysts	NCO indexes	Maximum core temperature (T_{max}) (°C)	Starting time at T_{max} [sec(min)]
DMCHA	100	120	360 (6:00)
	130	124	390 (6:30)
	150	130	435 (7:15)
Cu(tetraen)	100	124	390 (6:30)
	130	130	435 (7:15)
	150	134	450 (7:30)
Zn(tetraen)	100	126	420 (7:00)
	130	128	450 (7:30)
	150	131	495 (8:15)
Cu(tetraen):Zn(tetraen)	100	124	405 (6:45)
	130	131	435 (7:15)
	150	134	465 (7:45)
Cu(tetraen)-W	100	125	375 (6:15)
	130	131	405 (6:45)
	150	135	435 (7:15)
Zn(tetraen)-W	100	126	405 (6:45)
	130	128	435 (7:15)
	150	132	465 (7:45)
Cu(tetraen):Zn(tetraen)-W	100	125	375 (6:15)
	130	131	435 (7:15)
	150	134	450 (7:30)

4.3.8 NCO Conversion of Rigid Polyurethane Foams (RPUR Foams)

FTIR spectra of PMDI, polyol and RPUR foams are shown in Figures 4.25-4.27. The main wavenumbers of RPUR foam absorbance are shown in Table 4.15. The peaks at 2277 cm^{-1} (NCO), 1595 cm^{-1} (Ar-H), 1415 cm^{-1} (PIR) and 1220 cm^{-1} (PUR) were used in the calculation of NCO conversion [11, 12]. The calculation method of NCO conversion is shown in Appendix A. The goal of ATR-FTIR study was to determine the effect of NCO indexes on NCO conversion. The results demonstrated that NCO conversion decreased with increasing of NCO indexes. Polyisocyanurate (PIR) formation increased with increasing NCO indexes because the increasing of isocyanate resulted in trimerization. Figure 4.28 shows that more unreacted isocyante (2273 cm^{-1}) at the NCO index of 180 is observed since M(tetraen) catalysts were not specific toward of isocyanurate formation. RPUR foams catalyzed by metal complexes showed NCO conversion and PIR/PUR similar to RPUR foams prepared by DMCHA. The results are shown in Table 4.16.

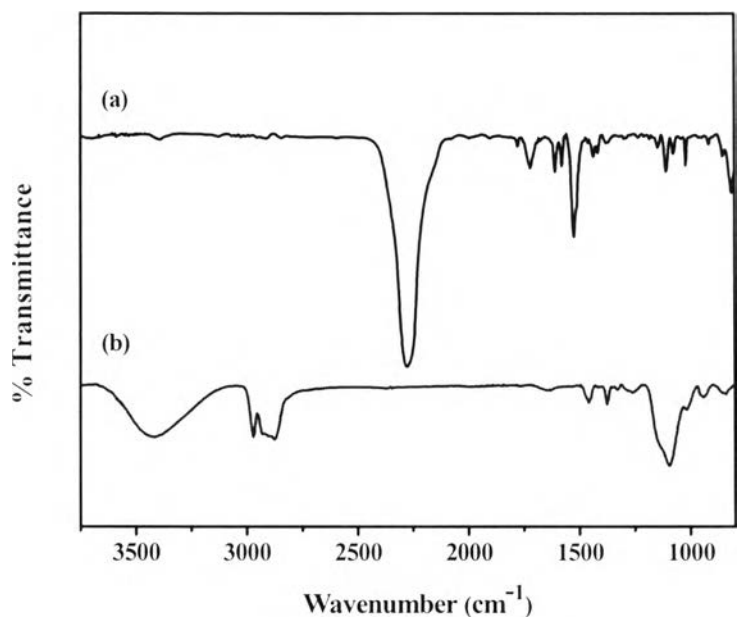

Figure 4.25 FITR spectra of starting materials (a) PMDI; (b) polyol

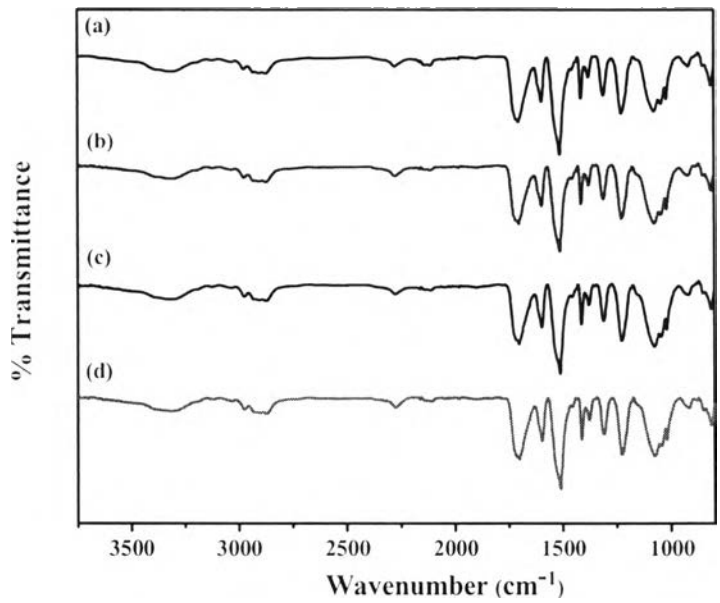

Figure 4.26 FTIR spectra of RPUR foams prepared at the NCO index of 100 and catalyzed by (a) DMCHA; (b) Cu(tetraen); (c) Zn(tetraen); (d) Cu(tetraen):Zn(tetraen)

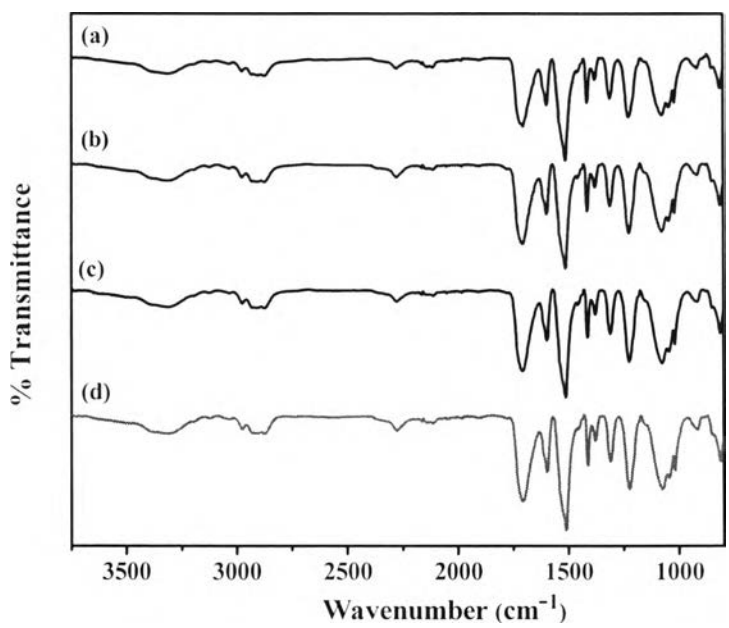

Figure 4.27 FTIR spectra of RPUR foams prepared at the NCO index of 100 and catalyzed by (a) DMCHA; (b) Cu(tetraen)-W; (c) Zn(tetraen)-W; (d) Cu(tetraen):Zn(tetraen)-W

Table 4.15 Wavenumbers of RPUR foam absorbance [34, 35]

Wavenumber (cm^{-1})	Chemical bond
2274-2275	N=C=O asymmetric stretching (isocyanate)
1702-1735	C=O stretching (urethane, urea, allophanate and biuret)
1594-1595	Ar-H (phenyl)
1509-1510	N-H bending (urethane)
1410-1411	C-N stretching (isocyanurate)
1373	C-N (uretoneimine)
1222	C-O stretching (urethane)

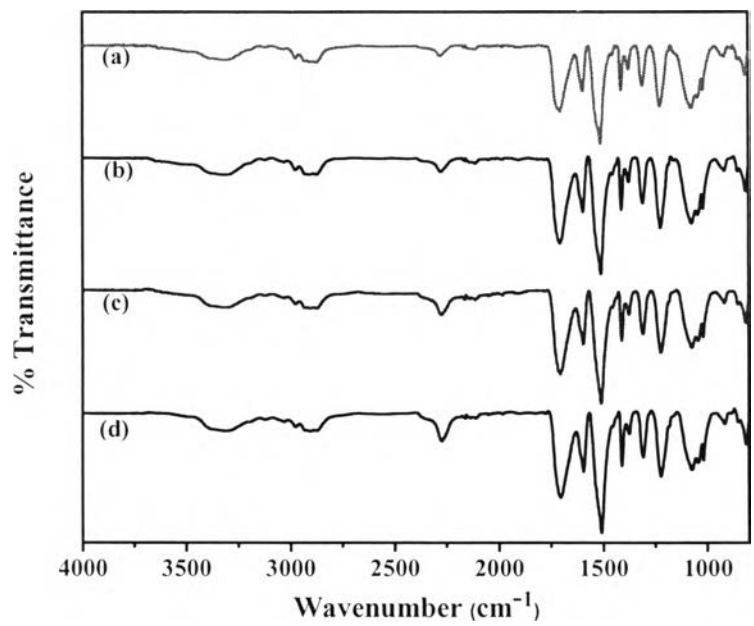

Figure 4.28 FTIR spectra of RPUR foams prepared at the different of NCO indexes (a) 100; (b) 130; (c) 150; (d) 180 and catalyzed by Cu(tetraen):Zn(tetraen)

Table 4.16 NCO conversion of RPUR foams prepared at the NCO indexes of 100-180

Catalysts	NCO indexes	NCO conversion (%)	PIR/PUR
DMCHA (ref.)	100	99.8	0.191
	130	99.5	0.210
	150	99.4	0.268
	180	99.0	0.311
Cu(tetraen)	100	99.7	0.189
	130	99.6	0.209
	150	99.3	0.220
	180	98.9	0.280
Zn(tetraen)	100	99.8	0.193
	130	99.8	0.203
	150	99.4	0.207
	180	98.9	0.283
Cu(tetraen):Zn(tetraen)	100	99.7	0.192
	130	99.5	0.204
	150	99.2	0.216
	180	98.8	0.289
Cu(tetraen)-W	100	99.7	0.173
	130	99.6	0.190
	150	99.3	0.217
	180	99.0	0.278
Zn(tetraen)-W	100	99.7	0.160
	130	99.5	0.200
	150	99.3	0.220
	180	98.9	0.274
Cu(tetraen):Zn(tetraen)-W	100	99.7	0.173
	130	99.5	0.205
	150	99.3	0.219
	180	90.0	0.254

4.3.9 Effect of NCO Indexes

Increasing of NCO indexes had an influence on density. Density of RPUR foams prepared by DMCHA and metal complexes synthesized in acetone and water are shown in Figures 4.29 and 4.30, respectively. The results revealed that the density of RPUR foams increased with increasing of NCO indexes since polymer matrix became more highly crosslinked [11]. RPUR foams prepared by DMCHA had the least density at all NCO indexes. RPUR foams catalyzed by metal complexes synthesized in acetone and water showed similar density. All metal complexes gave RPUR foams prepared at the NCO indexes of 100-150 with suitable density in the range of 40-50 kg/m^3. Reaction times and their S.D. are shown in Tables B14-B20 (Appendix B).

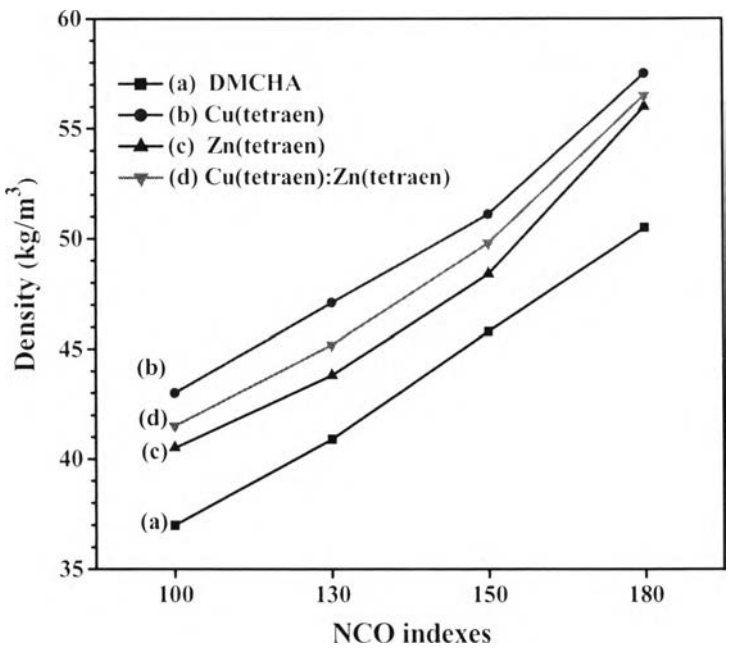

Figure 4.29 Effect of NCO indexes on density of RPUR foams prepared at the NCO indexes of 100-180 and catalyzed by (a) DMCHA (b) Cu(tetraen); (c) Zn(tetraen); (d) Cu(tetraen):Zn(tetraen)

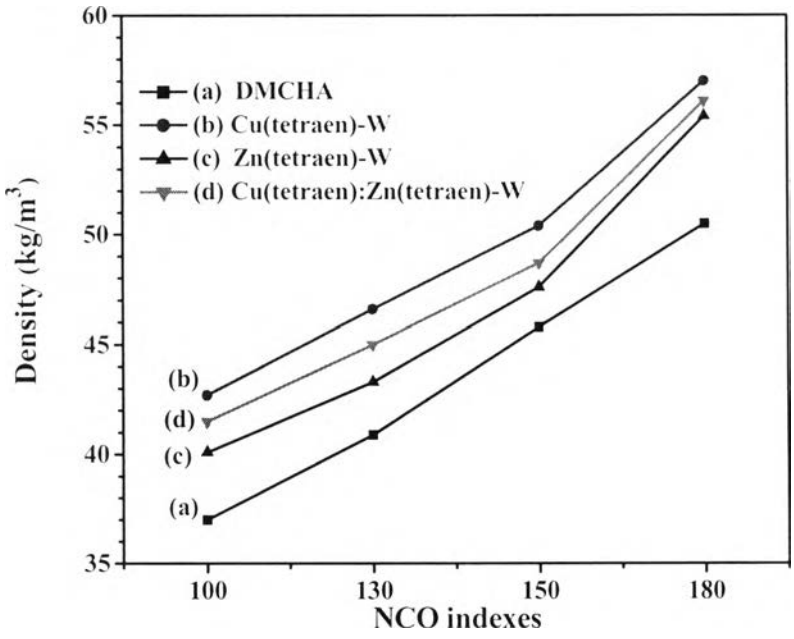

Figure 4.30 Effect of NCO indexes on density of RPUR foams prepared at the NCO indexes of 100-180 and catalyzed by (a) DMCHA; (b) Cu(tetraen)-W; (c) Zn(tetraen)-W; (d) Cu(tetraen):Zn(tetraen)-W

4.3.10 Compressive Strength

4.3.10.1 Compressive Strength of RPUR Foams Catalyzed by Different Catalysts

Parallel compressive strength of RPUR foams at the NCO index of 150 catalyzed by different catalysts was presented in Figure 4.31. It was indicated that RPUR foams prepared by metal complexes showed higher compressive strength than those prepared by DMCHA. Moreover, compressive strength corresponded with density of RPUR foams. The data are shown in Tables B14-B17 (Appendix B).

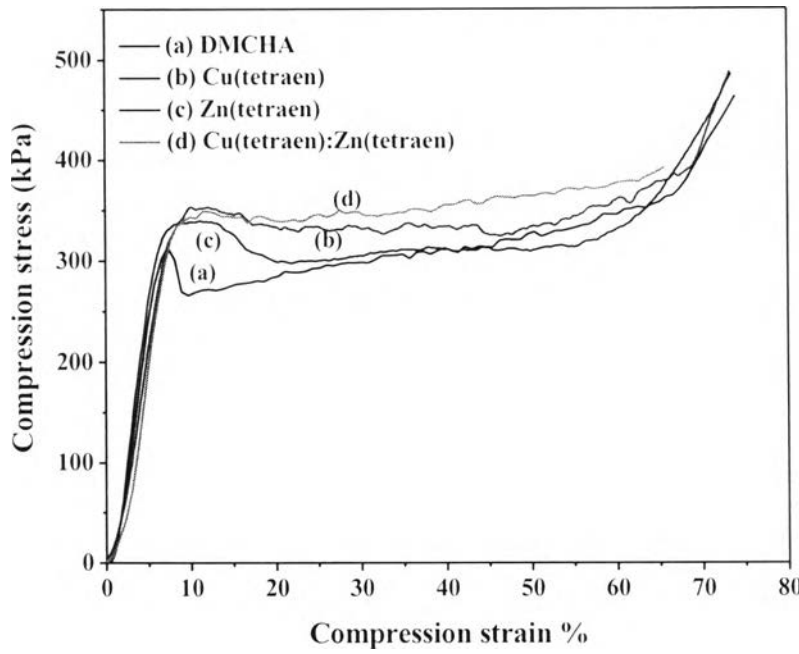

Figure 4.31 Compressive strength of RPUR foams prepared at the NCO index of 150 and catalyzed by (a) DMCHA; (b) Cu(tetraen); (c) Zn(tetraen); (d) Cu(tetraen):Zn(tetraen)

4.3.10.2 Effect of NCO Indexes on Compressive Strength of RPUR Foams

Parallel compressive strength of RPUR foams at the NCO indexes of 100, 150 and 180 is shown in Figure 4.32. RPUR foams prepared at the NCO index of 180 showed higher compressive strength than those prepared at the NCO indexes of 100 and 150. The results indicated that compressive strength is strictly related to NCO index since the polymer matrix became more highly crosslinked. As shown in Figure 4.29, NCO indexes were also related with density of RPUR foams, therefore, compressive strength increased with increasing of NCO indexes and density. RPUR foams catalyzed by Cu(tetraen):Zn(tetraen) showed higher compressive strength than that prepared from DMCHA.

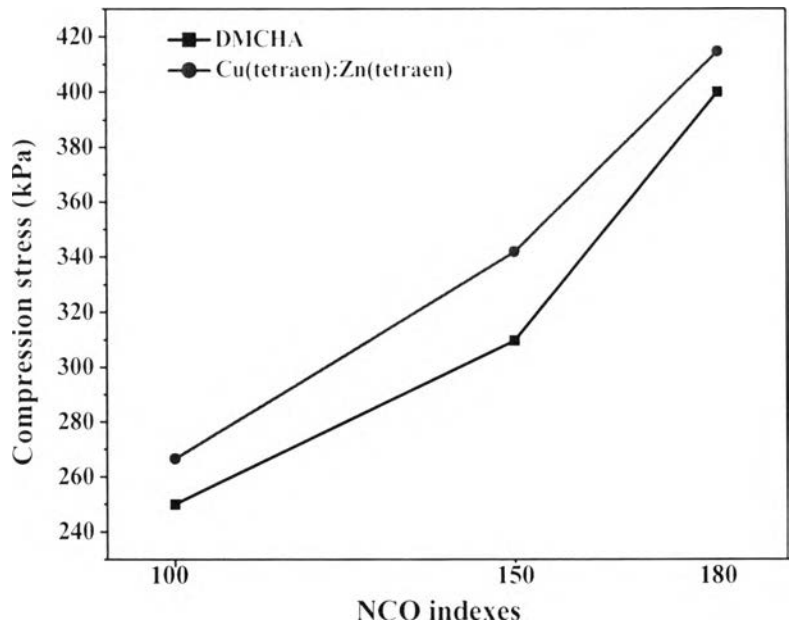

Figure 4.32 Effect of parallel compressive strength of RPUR foams prepared at the NCO indexes of 100-180 and catalyzed by DMCHA; Cu(tetraen):Zn(tetraen)

4.3.10.3 Effect of Blowing Agent on Compressive Strength

Parallel compressive strength of RPUR foams with different blowing agent content is shown in Figure 4.33. When the blowing agent content was increased from 1 to 4 pbw, the compressive strength of RPUR foams prepared by Cu(tetraen):Zn(tetraen) decreased from 419.8 to 173.3 kPa. It is generally known that the mechanical properties of the RPUR foams mainly depend on its density. According to the effect of blowing agent on RPUR foams density, the density of RPUR foams decreased with increasing of water content. The increasing of blowing agent generated more gas bubbles [36, 37]. Therefore, the compressive strength of RPUR foams decreased with the increase of water content. Reaction times and their S.D. are shown in Table B21 (Appendix B).

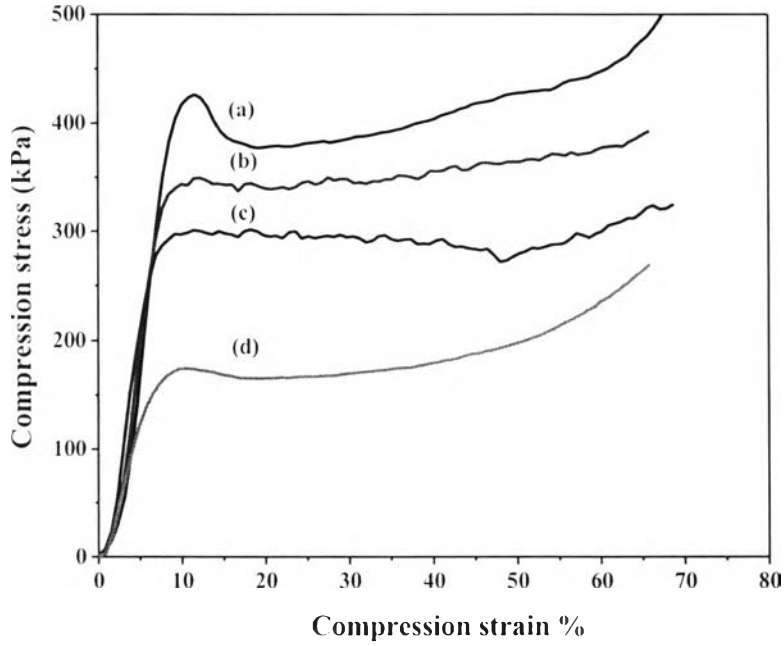

Figure 4.33 Effect of blowing agent content on compressive strength of RPUR foams prepared at the NCO index of 150 and catalyzed by Cu(tetraen):Zn(tetraen) (a) 1 pbw; (b) 2 pbw; (c) 3 pbw; (d) 4 pbw

4.3.10.4 Effect of Foam Rising Direction on Compressive Strength

Effect of foam rising direction on compressive strength is shown in Figure 4.34. It was found that the compressive strength in parallel direction was higher than that in perpendicular direction [38]. For the compression in parallel direction, the compression stress-strain curve relationship exhibited an initial linear rise corresponding to uniform elastic compression, followed by a protracted post-yield plateau, whereby the collapse of cells spread through the structure. A prominent curve in Figure 4.34(a) showed the drop in stress at the beginning of the plateau phase as a strain softening. Response to compression perpendicular to parallel direction was different. No plateau phase and no strain softening curves were observed. The stress initially increased linearly to the yield point, which showed lower than that parallel direction. This form of mechanical facilitated the application of foam materials to damage mitigation. The

differences in response for the two directions indicated the foam rising direction had an influence on the mechanical properties of RPUR foams [39-40].

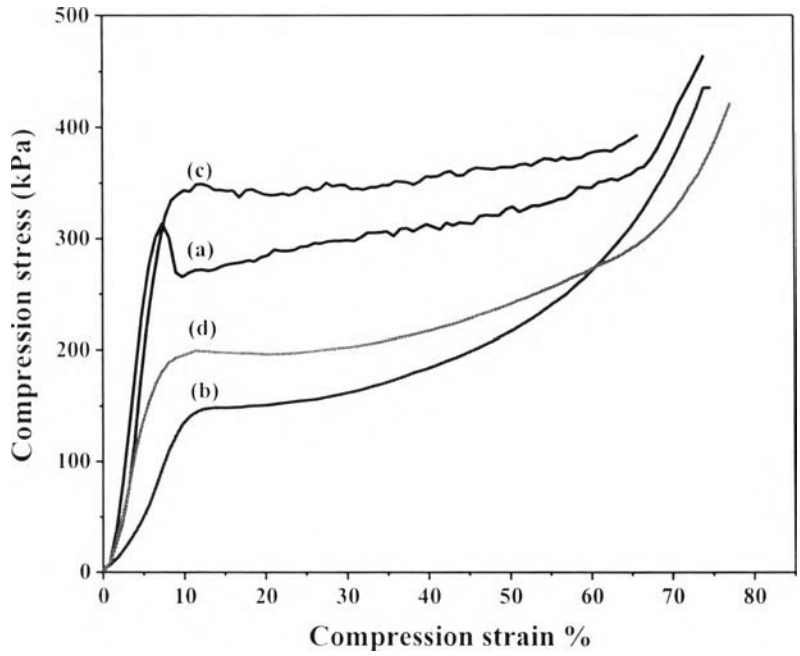

Figure 4.34 Compressive strength of RPUR foams prepared at the NCO index of 150 catalyzed by (a) DMCHA, parallel direction; (b) DMCHA, perpendicular direction; (c) Cu(tetraen):Zn(tetraen), parallel direction (d) Cu(tetraen):Zn(tetraen), perpendicular direction

4.3.11 Rigid Polyurethane Foams (RPUR Foams) Morphology

4.3.11.1 Morphology of RPUR Foams Synthesized by Different Catalysts

SEM of RPUR foams synthesized by different catalysts are presented in Figure 4.35. It was indicated that the cell morphology showed substantially closed. The RPUR foam prepared from DMCHA had an average cell size of 442.2 μm whereas the RPUR foams accelerated by Cu(tetraen), Zn(tetraen) and Cu(tetraen):Zntetraen) had average cell size of 465.3, 491.4 and 438.1μm, respectively.

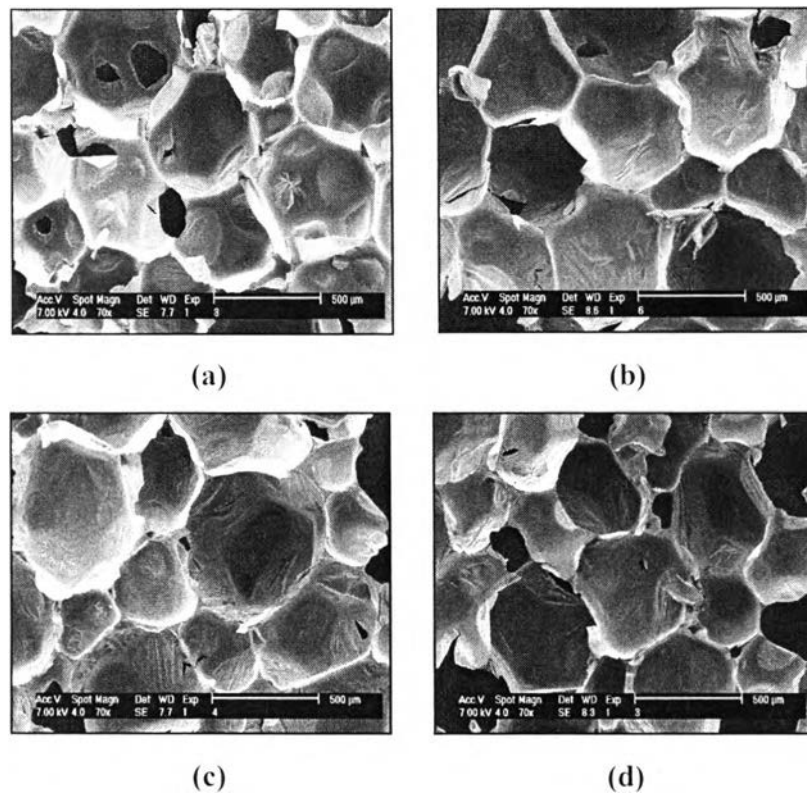

Figure 4.35 SEM of RPUR foams prepared at the NCO index of 150 and catalyzed by (a) DMCHA; (b) Cu(tetraen); (c) Zn(tetraen); (d) Cu(tetraen):Zn(tetraen)

4.3.11.2 Effect of Blowing Agent on Morphology of RPUR Foams

The surfaces of RPUR foams in parallel direction observed with SEM are reported in Figure 4.36. The average cell size of RPUR foams increased from 370.2 to 521.3 μm with the increase of water content from 1 to 3.0 pbw, respectively. The reaction of water with isocyanates generated carbon dioxide gas and exothermic heat. Since the increase of temperature of the reaction's mixture, the concentration of blowing gas in the mixture exceeded and a nucleation of bubbles began. During the foam rising, the already formed bubbles grew and new bubbles nucleated [41]. The increase of blowing agent content produced more bubbles. Therefore, the average cell size of RPUR foams increased with the increase of water content [42].

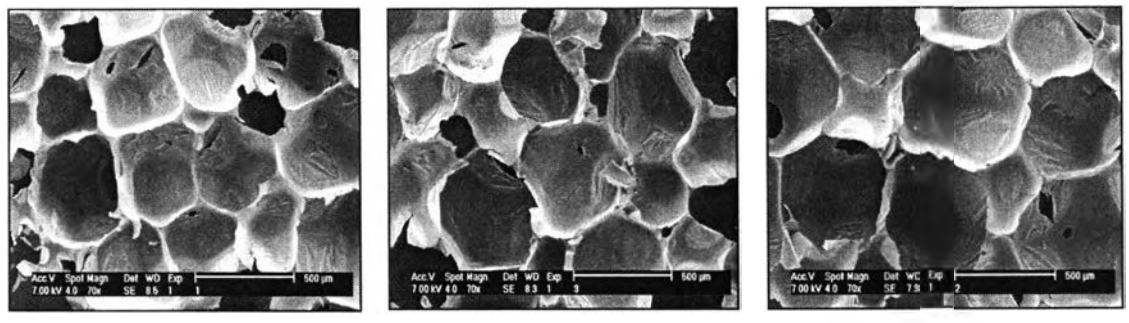

(a) (b) (c)

Figure 4.36 SEM of RPUR foams prepared at the NCO index of 150 and catalyzed by Cu(tetraen):Zn(tetraen) with different blowing agent content (a) 1 pbw; (b) 2 pbw; (c) 3pbw

4.3.11.3 Effect of Foam Rising Direction on Morphology of RPUR Foams

Scanning electron micrographs (SEM) of RPUR foams prepared by Cu(tetraen):Zn(tetraen) is shown in Figure 4.37. The cell structures of Figure 4.37(a) which rose in parallel direction had more spherical than that perpendicular direction (Figure 4.37(b)). The cell morphology in perpendicular direction of foam rising usually had aspect ratio more than 1. Aspect ratio could be calculated by the ratio of the diameters of the major and minor ellipse axes [17]. Therefore, the direction of foams rising was related to mechanical properties (Figure 4.34).

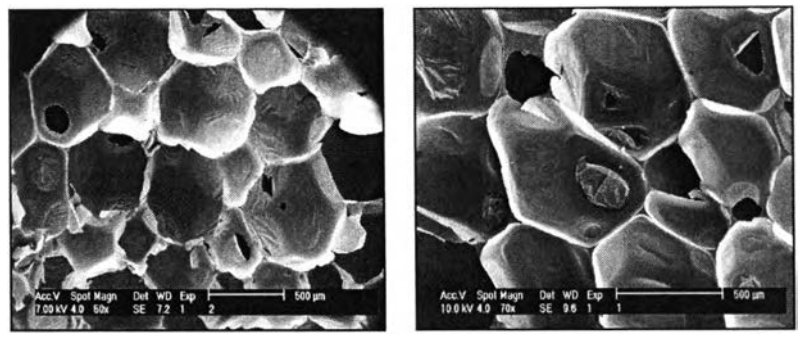

(a) (b)

Figure 4.37 SEM of RPUR foams prepared at the NCO index of 150 and catalyzed by (a) Cu(tetraen):Zn(tetraen), parallel direction; (b) Cu(tetraen):Zn(tetraen), perpendicular direction

4.3.12 Thermal Stability

4.3.12.1 Thermogravimetric Analysis (TGA) of RPUR Foams

RPUR foams are mainly used as heat insulating materials and their thermal behavior is very important. Thermal decomposition was investigated by thermogravimetric analysis (TGA). Figure 4.38 and Table 4.17 show TGA data of RPUR foams catalyzed by DMCHA, Cu(tetraen), Zn(tetraen) and Cu(tetraen):Zn(tetraen) prepared at the NCO index of 150. It was found that the initial decomposition temperature (IDT) ranged from 278 to 287 °C for 5 to 6% of foam weight loss. The initial decomposition temperature related to the decomposition of urethane [43, 44]. The maximum decomposition temperature (T_{max}) was recorded at 344 to 349 °C. The foams prepared from metal complexes showed similar thermal stability to that of DMCHA.

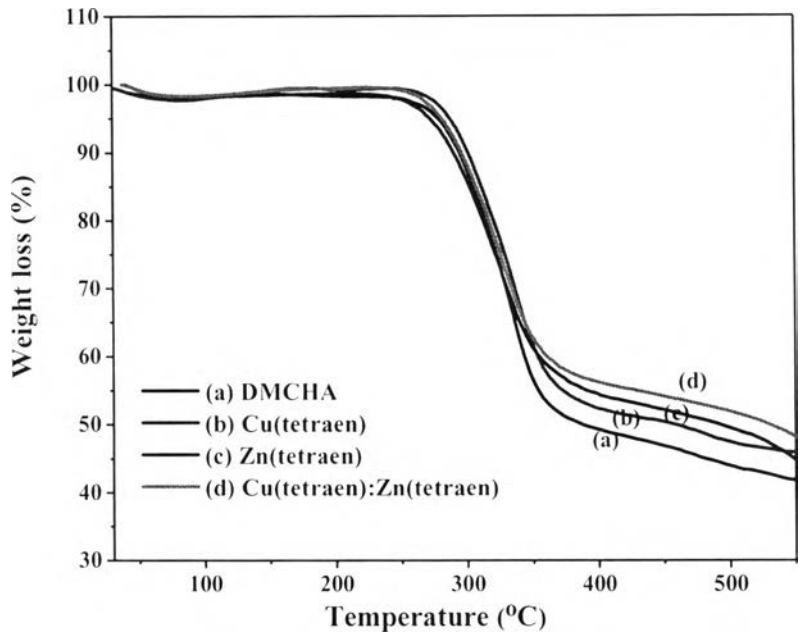

Figure 4.38 TGA thermograms of RPUR foams prepared at the NCO index of 150 and catalyzed by (a) DMCHA; (b) Cu(tetraen); (c) Zn(tetraen); (d) Cu(tetraen):Zn(tetraen)

Table 4.17 TGA data of RPUR foams prepared at the NCO index of 150 and catalyzed by different catalysts

Catalysts	Initial decomposition temperature (°C)	%Weight loss at initial decomposition temperature	Maximum decomposition temperature (°C)
DMCHA	282.6	5.4	344.1
Cu(tetraen)	287.5	5.1	349.8
Zn(tetraen)	278.7	6.2	348.2
Cu(tetraen):Zn(tetraen)	283.1	5.3	343.8

4.3.12.2 Thermal Conductivity

Thermal conductivity of RPUR foams depends on cell size, foam density and on thermal conductivity of gases (blowing agent). These foams have closed cells which trap carbon dioxide and air [45, 46]. Table 4.18 shows thermal conductivity of RPUR foams catalyzed by DMCHA and Cu(tetraen):Zn(tetraen). It was found that they showed similar thermal conductivity.

Table 4.18 Thermal conductivity of RPUR foams prepared the NCO index of 150

Catalysts	Thermal conductivity (W/mW)	Standard deviation
DMCHA	0.0366	0.0001
Cu(tetraen):Zn(tetraen)	0.0374	0.0002

4.3.13 External Appearance of Rigid Polyurethane Foams (RPUR Foams)

External appearance of RPUR foams catalyzed by non-catalyst, tetraen and $Cu(OAc)_2$ was shown in Figure 4.39. It was found that the foams showed undesirable appearance. Therefore, use of metal complex catalyst is necessary for accelerating urethane reaction. Reaction times, volume and density of RPUR foams catalyzed by non-catalyst, tetraen and $Cu(OAc)_2$ were compared with those catalyzed by metal complexes (Table 4.19).

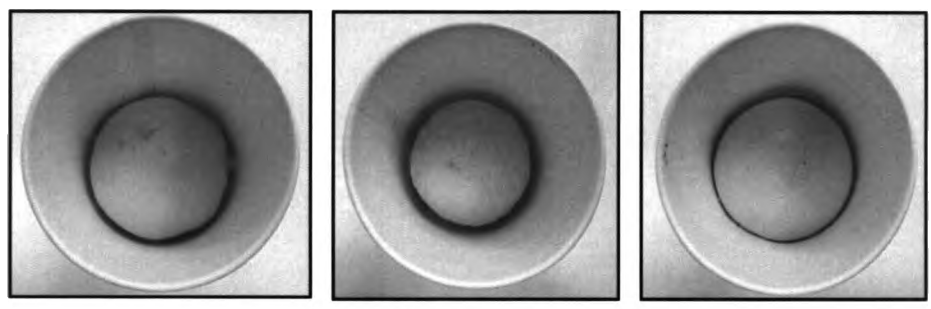

Figure 4.39 External appearance of RPUR foams prepared at the NCO index of 100 and catalyzed by (a) non-catalyst; (b) tetraen; (c) $Cu(OAc)_2$

Table 4.19 Comparison of RPUR foams catalyzed by non-catalyst, tetraen, $Cu(OAc)_2$ and metal complexes prepared at the NCO index of 100

Catalysts	Cream time (min)	Gel time (min)	Rise time (min)	Tack free time (min)	Density (kg/m^3)	Volume (V/8)
non-catalyst	1:55	2:48	15:22	23:20	62.1	4.00
Tetraen	1:45	2:33	16:45	18:40	-	4.00
$Cu(OAc)_2$	1:18	2:45	13:37	17:52	59.2	4.50
Cu(tetraen)	0:35	1:09	3:52	3:40	43.0	6.25
Zn(tetraen)	0:33	1:32	5:44	6:00	40.5	6.50
Cu(tetraen):Zn(tetraen)	0:35	1:16	4:40	4:26	41.8	6.50

External appearance of RPUR foams in the molds was shown below. Figure 4.40 (a)-(d) and 4.40 (e) presented RPUR foams prepared in cylinder mold and cubic mold, respectively. It was indicated that RPUR foams catalyzed by metal complexes could be prepared in different mold sizes.

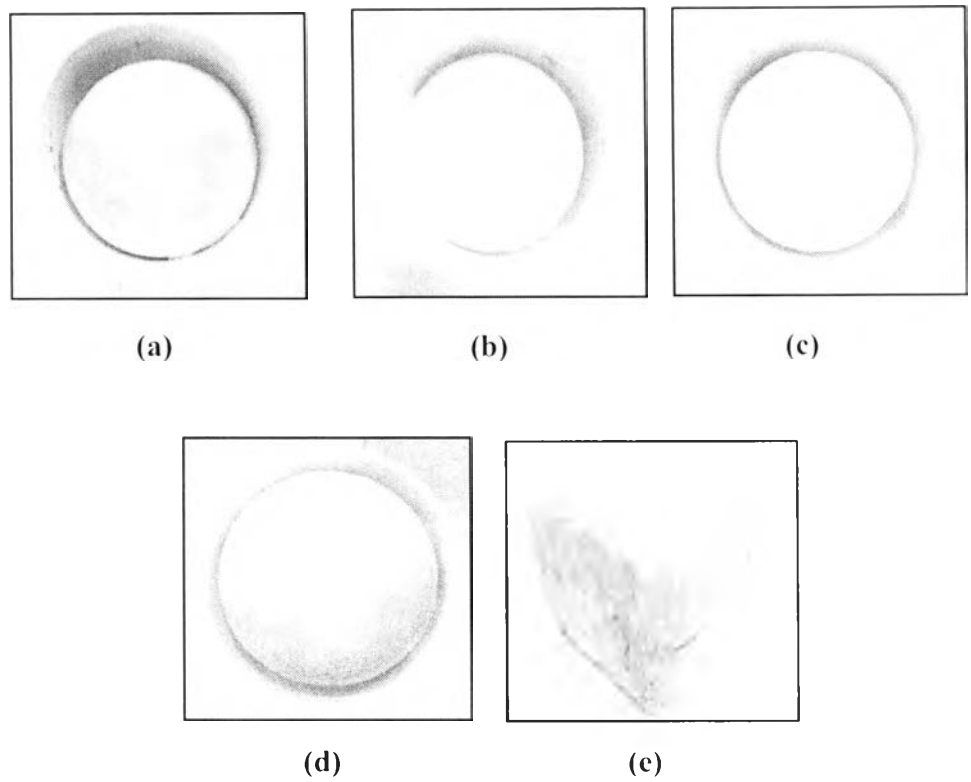

Figure 4.40 External appearance of RPUR foams prepared at the NCO index of 150 and catalyzed by (a) Cu(tetraen); (b) Zn(tetraen); (c) Cu(tetraen):Zn(tetraen); (d) DMCHA (cylinder mold); (e) Cu(tetraen):Zn(tetraen) (cubic mold)